SCUOLA DI SCIENZE

Dipartimento di Chimica Industriale“Toso Montanari”

Corso di Studio in

Chimica Industriale

Classe L-27- Scienze e Tecnologie Chimiche

Study of Co-based hydrotalcite-derived mixed metal oxides partially modified with silver as potential catalysts for N_2O decomposition

CANDIDATO
Lorenzo Buselli

RELATORE
Chiar.mo Prof. Fabrizio Cavani

CORRELATORI
Dott.ssa Magdalena Jabłońska

Prof.ssa Regina Palkovits

Anno Accademico 2015-2016

Acknowledgements

Firstly, I want to thank Prof. Regina Palkovits, for the opportunity to work in her research group, the ITMC, and my supervisor Prof. Cavani. I want to thank my supervisor in Aachen Magda, who helped and supported me during my internship, and let me grow up under many viewpoints. Then, I want to thank all the people that I met in Germany: my lab and office colleagues, my little Italian team Christian and Francesca, my flatmates Alex and Pippo, and all my other friends who made me feel like at home.

Tengo particolarmente a ringraziare tutti coloro che mi hanno accompagnato durante il mio percorso universitario, da Pisa a Bologna: la mia famiglia di Via Fiorentina 54, poi Togno, Solve, Vanessa e tutti coloro con cui ho condiviso qualcosa a Pisa. Spostandoci in Emilia, voglio ringraziare miei compagni di corso e di laboratorio, il buon Molly, i miei amici siculi-e non, concludendo con i ragazzi del Due Torri.

Un doveroso ringraziamento va a tutti i miei amici piombinesi, con i quali mi sentirei in famiglia anche qualora dovesse passare un secolo tra una visita e l'altra.

Per finire, grazie alla mia famiglia che rappresenta le fondamenta di tutto quello che sto costruendo, e al mio amore Ludovica, che è sempre qui, accanto a me.

Grazie a tutti

Thank you

Dankeschön

The Erasmus + project is acknowledged for the opportunity to do my exchange and for the financial support.

Acronym list

deN$_2$O: decomposition of N$_2$O

deNO$_x$: reduction of NO$_x$

HT-l compounds:hHydrotalcite-like compounds

XRD: X-ray diffraction.

TGA: thermogravimetric analysis

BET: Brunauer-Emmett-Teller method

H$_2$-TPR: hydrogen temperature-programmed reduction

XPS: X-ray photoelectron spectroscopy

IR: infrared

WHSV: weight hourly space velocity

Catalysts code:

- CHT-Co$_x$Al$_y$: mixed metal oxides obtained by calcination of HT-l compounds with molar ratio of Co/Al = x/y
- TD-Co$_x$Al$_y$: mixed metal oxides obtained by thermal decomposition with molar ratio of Co/Al = x/y
- (X wt.% Ag)CHT-Co$_x$Al$_y$: mixed metal oxides obtained by calcination of HT-l compounds with molar ratio of Co/Al = x/y, and subsequently modified with X wt.% of Ag

Contents

Chapter 1: Introduction

This chapter describes the environmental problems associated with N_2O and its possible abatement through catalytic decomposition of N_2O over hydrotalcite-derived mixed metal oxides, and in particular silver-doped materials.

1.1 N_2O as greenhouse and ozone layer depleting gas

Nitrous oxide, also known as laughing gas, has been discovered (1772) by Joseph Priestley. The British chemist used the experimental apparatus designed by Stephen Hales, to discover a host of gases, including N_2O, which he called “nitrous air, diminished”.[1] Humphrey Davy initiated the applications of N_2O as anaesthetic, because he noticed the exhilaration effect of nitrous oxide mixed with a certain amount of oxygen. Furthermore, Kenneth M. Swezey published in *Popular science* (1949) an article with the instruction for the synthesis of N_2O dedicated for young scientists (Fig. 1.)..[2]

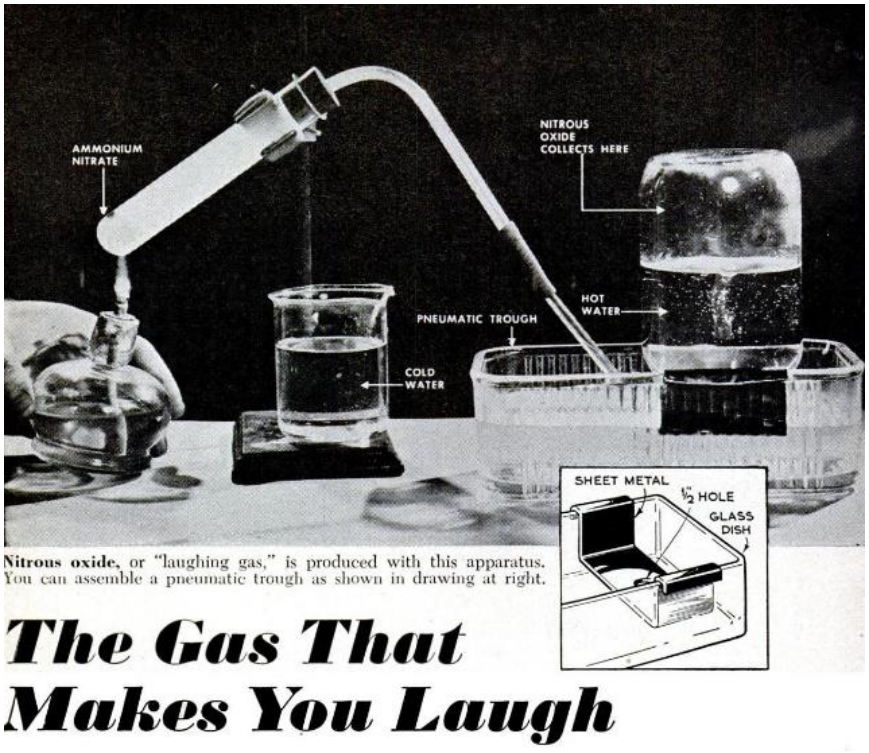

Fig. 1 Apparatus for N_2O production (Popular Science, 1949, 154, 236-238)

Afterwards, the physicochemical properties of N_2O was recognized and published. Under the normal condition nitrous oxide is a colourless gas, with a typical pleasant week smell and a sweet taste. The molecule is slightly polar (μ=0.17) and it has a linear asymmetric structure, with a bond lengths of N-N 1.126Å and N-O 1.186Å, and two resonance structures (Fig. 2.).[3]

Fig. 2 Resonance structures of N_2O

N_2O has been present in the atmosphere since life on heart had begun, and its concentration did not change appreciably for thousands of years. The concentration of N_2O in atmosphere started to increase rapidly from around 1850, and much more dramatically from 1950 (in parallel with the increase in global population and industrialization) (Fig. 3.).[4]

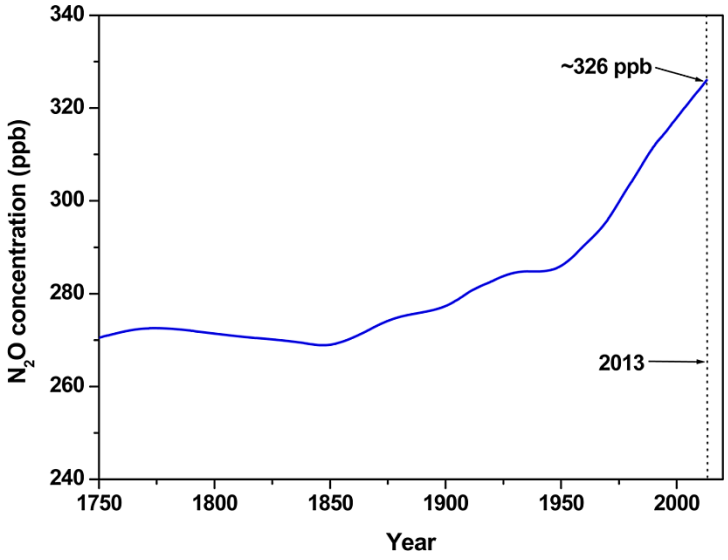

Fig. 3 General trend of atmospheric N_2O concentration in the atmosphere (ACS Catal. 5, 6397–6421 (2015))

The main N_2O sources are natural processes in lands and oceans. However, for N_2O increase is also related to the anthropogenic sources, such as fertilizers use, biomass burning, combustion of fossil fuels, industrial activities (especially adipic acid and nitric acid production) and wastewater treatment, etc.[5]

Due to significant increase of N_2O concentration over years the Third Conference of the Parties (COP-3) UN Framework Convention on Climate Change in Kyoto (1997), approved N_2O as one of the most dangerous greenhouse gas emission among CO_2, CH_4, HFCs, PFCs, SF_6. N_2O is considered as the third most important greenhouse gas (after CO_2 and CH_4) due to its long lifetime in atmosphere (114 years), leading to a Global Warming Potential (GWP) of approximately 310 times higher compared to CO_2.[4–6] Furthermore, N_2O is the most important stratospheric-ozone-depleting substance, which depletes the stratospheric ozone in a way similar to CFCs and other ozone-depleting halocarbons. Nevertheless, N_2O emissions are not regulated by Montreal protocol,[4] which is the international treaty designed to protect the ozone layer by controlling the emissions of the ozone depleting substances. Consequently, the control of N_2O emissions has been one of the biggest environmental challenge of the last twenty years.

1.2 Catalytic decomposition of N_2O

N_2O emissions abatement can be generally achieved in two different ways by:

(i) limiting the formation of N_2O,

(ii) employing after-treatment technologies.

Concerning the emission of N_2O from the agricultural sector - the major anthropogenic sources - the first approach is the best solution. On the other hand, regarding the control of N_2O emission from combustion and industrial sources, the employment of end-of-pipe remediation technologies is the most feasible way.[5] In general two ways for N_2O abatement are promising form practical and economical point of view:

(i) N_2O decomposition,

(ii) N_2O reduction with CO, NH_3, etc.

One of the biggest advantages of N_2O decomposition (deN_2O) is the fact that there is no need for additional co-feeding of other gases. Such simplicity led to application of deN_2O in adipic or nitric acid production plants, which are the main N_2O industrial sources. During nitric acid production, N_2O is formed as an undesired by-product in the catalytic oxidation of ammonia over the Pt–Rh gauzes. The possible locations for N_2O abatement technologies are marked in a typical flowsheet of a dual-pressure nitric acid plant (Fig. 4.):[7,8]

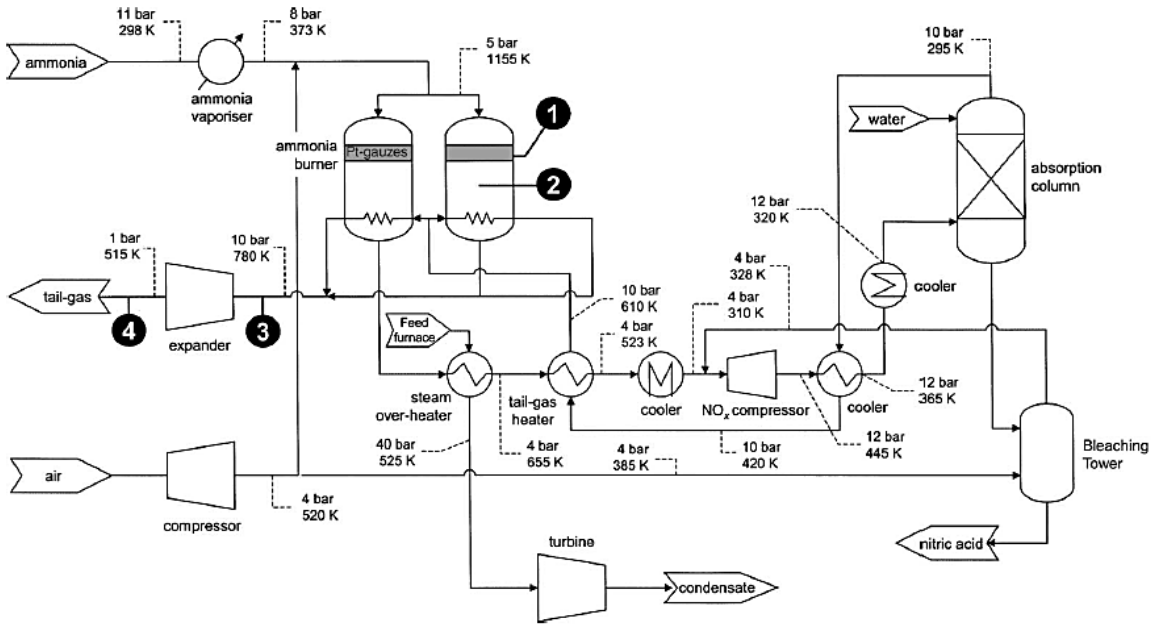

Fig. 4 Flowsheet of a dual pressure nitric acid production plant (Applied Catalysis B: Environmental 44 (2003) 117–151)

The primary and secondary possible abatement points concern respectively a modification in the ammonia oxidation catalyst or in the high-temperature zone immediately downstream of the ammonia burner. While the first one is economically unfeasible (the catalytic conversion process is already one of the most efficient processes known), the second one requires extreme thermally stable catalysts. Thus, low temperature applications of catalytic deN_2O technologies: ternary (upstream of the expander) or quaternary (downstream of the expander) abatement, seem to be interesting alternatives.

N_2O decomposition is an exothermic reaction, but it presents kinetic restriction at low temperature (pure nitrous oxide is stable up to 500 °C, at atmospheric pressure) (Eq. 1):[3,9]

$$2N_2O \rightarrow 2N_2 + O_2 \qquad \Delta H^0 (25°C): 163\ KJ/mol \qquad (1)$$

The catalytic deN_2O involves the adsorption of N_2O at the active centres, followed by its dissociation in a nitrogen molecule and a surface oxygen one. The last step is the regeneration of the active site (*) by recombination of two surface oxygen molecules or by direct reaction between a surface oxygen species and another molecule of N_2O[9] (Eq. 2-5):

$$N_2O + * \rightarrow N_2O* \qquad (2)$$

$$N_2O \rightarrow N_{2(g)} + O* \qquad (3)$$

$$O* + O* \rightarrow O_{2(g)} + 2* \qquad (4)$$

$$N_2O + O* \rightarrow N_{2(g)} + O_{2(g)} + * \qquad (5)$$

The adsorption of N_2O takes place on an active metal ion, through electron-back donation from d metal orbitals to the antibonding π^* orbitals of N_2O. This lead to the destabilization of the N-O bond, and its consequent scission. The catalysts dedicated for deN_2O are required to donate electrons for the N_2O dissociative adsorption. They include metal surface, oxides with some local charge donation properties, isolated transition metals with multiple oxidation state, but also F-centres and coordinatively unsaturated sites in transition-metal-exchanged zeolites.[9,10] The regeneration of the catalyst surface can occur via Langmuir−Hinshelwood (LH) mechanism (Eq. 4) or Eley–Rideal (ER) mechanism (Eq. 5). For most of the catalysts, the desorption of $O_{2(g)}$ through recombination of two surface oxygen molecules is the rate-determining step of deN_2O. Therefore, also the oxygen mobility on the surface of the materials is a crucial parameter which limits the efficiency of deN_2O for several catalysts.[10–12]

A wide number of catalysts were tested for deN_2O, including:

(i) supported and unsupported metals,

(ii) pure and mixed metal oxides,

(iii) zeolite-based catalysts.

Most of the pointed catalysts are deactivated in the presence of O_2, H_2O, NO, SO_2, which appear in real exhausts. For example, O_2 can adsorb on the catalysts active sites, decreasing the number of available sites for N_2O. Therefore, potential catalysts need to maintain high catalytic activity also in real conditions.[9]

Among the catalysts presented in literature, rhodium-modified materials serve as one of the most active for deN_2O.[13–15] An important drawback of this group of catalysts is high price of rhodium nitrate (the most efficient precursor in deN_2O). However, silver-modified materials represent a promising alternative mainly due to the lower cost of metal precursor, as well as satisfying catalytic activity.[16–18] Mixed metal oxides represent a valid alternative to noble metal-modified materials, since they show satisfactory deN_2O activity and stability during reaction, and relative low price.[5] Mixed oxides prepared by thermal decomposition of hydrotalcite-like compounds (HT-l compounds), serve as one of the most attractive classes of mixed oxide-based catalysts for deN_2O. Starting from the work of Kannan *et al.*, several HT-derived mixed metal oxides with different compositions were tested for deN_2O, e.g. Cu-Al-O_x, Ni-Mg-Al-O_x, Co-Cu-Mg-Al-O_x, etc.

Although lots of efforts were already done in order to develop satisfactory catalysts for deN_2O, the challenges remain to find selective, stable, non-toxic, cheap and working at low-temperatures catalysts.

1.3 Hydrotalcite-like compounds

Hydrotalcite is a hydroxycarbonate of magnesium and aluminium that was first discovered in Sweden (1842). It is described with general formula $Mg_6Al_2CO_3(OH)_{16}\cdot 4(H_2O)$, and characterized by a typical layered structure similar to the octahedral brucite, $Mg(OH)_2$, but Mg^{2+} ions are partially replaced by Al^{3+} ions, leaving a positive charge in the layers. The charge is then compensate by carbonates anions, which lay in the interlayer space together with some water molecules.[19] The hydrotalcite-like compounds (HT-l compounds) correspond to the synthesized materials with general formula of:

$[M^{II}_{1-x}M^{III}_{x}(OH)_2]^{x+}\ (A^{n-}_{x/n})\cdot mH_2O$

where M^{II}: divalent metal, e.g. Mg, Ni, Zn, Fe, Co, Cu etc., M^{II}: trivalent metal, e.g. Al, Mn, Cr, Fe, Co etc., A: interlayer anion, e.g. Co_3^{2-}, NO_3^-, OH^-, etc., x is usually $0.20<x<0.34$ and m depends on the amount of water in the interlayer.[19,20] (Fig. 5).

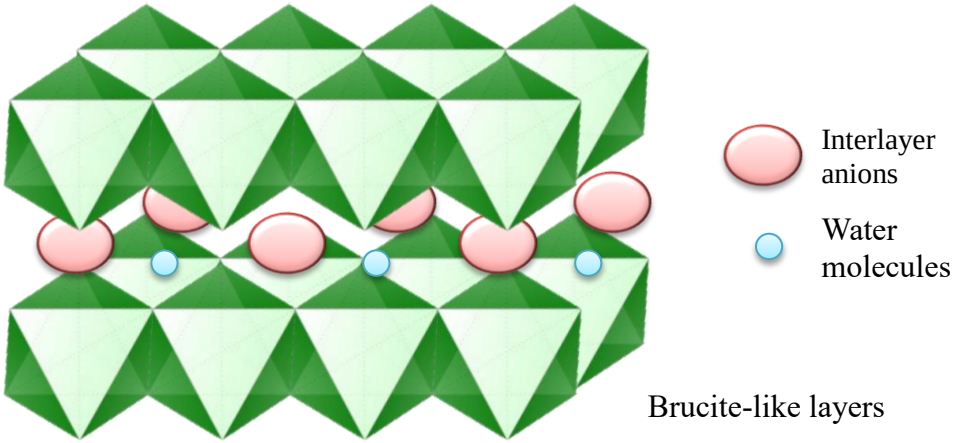

Fig. 5 Layered structure of an HT-l compound

Due to wide variety of possible cations and anions that can be introduced within the brucite-like layers it is possible to synthesize compounds with different compositions and stoichiometries. The cations with ionic radius similar to Mg^{2+}, e.g. (M^{2+} = Mg^{2+}, Fe^{2+}, Co^{2+}, Ni^{2+}, Cu^{2+}, Zn^{2+}, etc. or M^{3+} = Al^{3+}, Cr^{3+}, Mn^{3+}, Fe^{3+}, Co^{3+}, etc.) and almost all anions (not forming strong complex with the cations) can be applied to form HT-l compounds.[20]

The synthesis of HT-l compounds can be carried out by various methods:

(i) coprecipitation in alkaline conditions (the most common),

(ii) anion exchange,

(iii) hydrothermal synthesis,

(iv) sol-gel.

The calcination of HT-l compounds at temperature above 400°C leads to a dispersed mixed metals oxides with high specific surface area and synergetic effect among the elements due to the intimate interdispersion of the metal oxides. Furthermore, such low calcination temperatures of HT-l compounds allow reconstructing the HT-l structure by rehydration, when the calcined materials are put in contact with aqueous solutions containing various anions (so called *memory effect*). Due to their unique properties, these materials find application in many fields of catalysis. E.g. they are suitable catalysts for deN_2O, because of the great variety of elements that can be accommodated into the structure, the synergetic effect between different oxides homogeneously dispersed and their relative low price.

1.3.1 DeN_2O over hydrotalcite-derived mixed metal oxides

Recently, the catalytic deN_2O over HT-derived compounds was extensively reviewed by Jabłońska and Palkovits.[21] Kannan *et al* [22,23]. investigated several calcined HT-l compounds, combining various metals (M^{2+}: Mg, Co, Ni, Cu or Zn and M^{3+}: Al, Fe or Cr) and varying their M^{2+}/M^{3+} molar ratio. The first studies on the effect of the divalent cation underlined the superior catalytic activity of Co- or Ni-modified catalysts (Fig. 6):

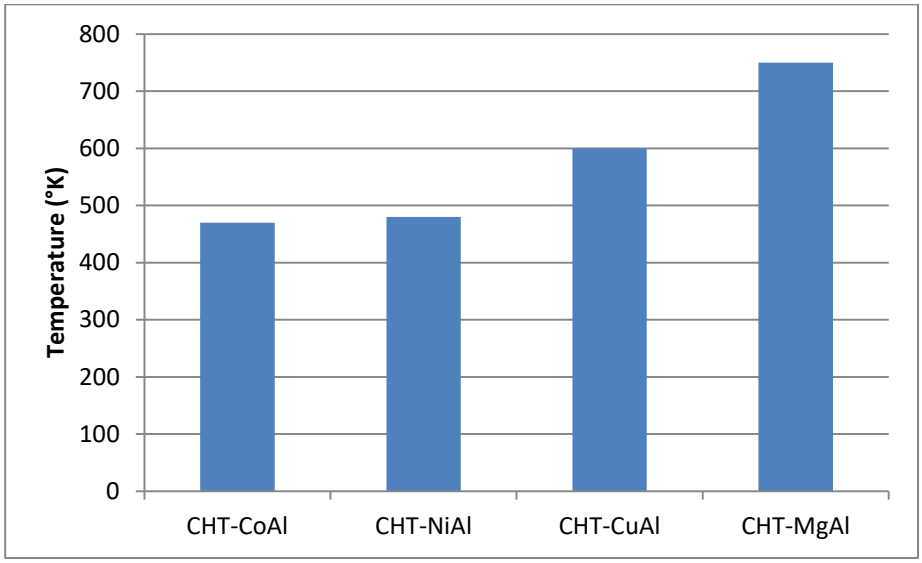

Fig. 6 Plot of temperature required for 50% conversion of N_2O over calcined HT-l compounds (Applied Clay Science 13 (1998) 347–362)

Cobalt- or nickel-doped catalytic systems provide a partial electron donation to the N_2O, which is a primary requirement for deN_2O. On the other hand, materials containing Mg and Zn are inactive due to their completely fill electronic configuration. The slightly higher activity of the Co-containing compounds was explained due to the weaker Co-O_{ads} bond compared to corresponding Ni-analogue. For Co-doped catalysts, after calcination of the precursors, only spinel phases were identified (Co_3O_4, $CoAl_2O_4$), with some oxygen defects. The good dispersion of cobalt oxide species on the surface of the materials and the presence of such defects are responsible for the high activity of these catalysts.

Among the trivalent cations (including Fe, Cr, Al), Al were reported for providing the highest activity, especially with cobalt-containing material (Co/Al = 3/1) (Fig. 7.).

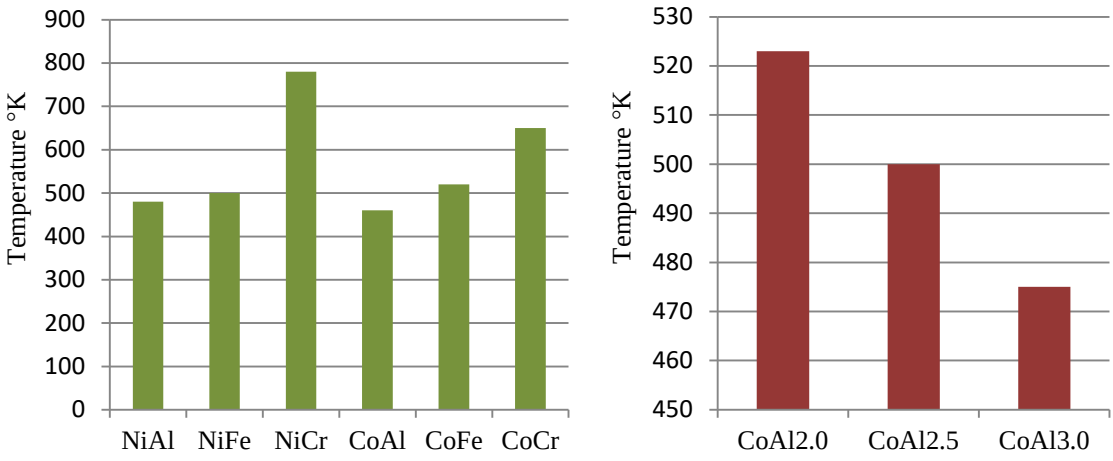

Fig. 7 Plot of temperature required for 50% conversion of N_2O over calcined HT-l compounds (Applied Clay Science 13 (1998) 347–362)

A synergetic effect of metal oxides can be obtained through the introduction of more than one divalent or trivalent cation within the HT-l structure, for example Cu-Co-Mg-Al-O_x as presented by Chmielaraz *et al.*[24]. The presence of copper, in fact, facilitates the electron transfer between Co and N_2O.Similarly, the enhanced activity after incorporation of small amount of copper into cobalt spinels for deN_2O was also reported by Franken *et al.*[25] The simultaneous presence of copper and cobalt, together with magnesium, leads to the formation of highly crystalline mixed spinels phases[26] ($MgAl_2O_4$, $CuAl_2O_4$, $CoAl_2O_4$, Co_3O_4, $Cu_xCo_{3-x}O_4$). These materials show synergetic interactions between copper and cobalt.

Pèrez-Ramirez *et al.*[27–29] studied the effect of magnesium loading on activity in deN_2O over calcined HT-l materials. MgO itself was proved to be inactive in deN_2O; however, Mg acts as a structural promoter for calcined Co-Al HT-l compounds, improving the textural properties of the materials, i.e. the introduction of magnesium give rise to smaller crystallite sizes and leads to higher specific surface areas. Furthermore, doping with Mg eliminates the initial deactivation of the catalysts in the presence of SO_2 and O_2.

Obalova *et al.*[30–32] investigated numerous combinations of Co-Mn-Al HT-derived mixed metal oxides, and reported promising activity (also in presence of O_2 and H_2O) for material with a Co:Mn:Al molar ratio of 4:1:1. Other authors obtained additional improvements on deN_2O activity, by doping Co-based calcined HT-l compounds with small amounts of promoters including:

(i) alkali metals (Li, Na, K), [33,34]

(ii) noble metals (Rh, Pd),[29,34,35]

(iii) rare earth metals Ce[36] and La[29,34],

which were introduced during coprecipitation or by impregnation with an aqueous solution containing the desired metal precursors. E.g. Pacultova *et al.*[37] tested a K-doped Co-Mn-Al-O_x (Co:Mn:Al = 4:1:1) for deN_2O in a pilot scale reactor at the bypassed tail gas from a nitric acid plant downstream. The authors reported an average value of N_2O conversion of about 90% at 450°C for 112 days.

1.4 Silver-based catalysts

Silver-doped materials are applied as catalysts for the selective oxidation of methanol, and the epoxidation of ethylene, or the removal of NO_x from exhaust gases [38–42]. An important characteristic of these studies – compared with other noble metal catalysts – is high deNO_x activity together with high N_2 selectivity (low N_2O formation). Silver-based catalysts were also investigated for the photocatalytic deN_2O,[43–46] as well as for the direct decomposition; however, these studies remain relatively scarce. Angelidis *et al*. and Tzitzios *et al.* [16,18,47] studied deN_2O over Ag-(Pd/Rh) supported on γ-Al_2O_3. Silver deposited on alumina showed poor catalytic activity, and suffered from strong oxygen inhibition (N_2O conversion decreased from 50% to 15% at 650°C in presence of O_2). The doping with Pd or Rh significantly enhanced the activity of the Ag/Al_2O_3 catalyst, even in presence of O_2. The highest activity showed by 5 wt.%Ag-3 wt.%Pd/γ-Al_2O_3 and 5 wt.%Ag-0.05 wt.%Rh/γ-Al_2O_3, revealed a synergetic effect between the deposited metals. Kumar *et al.*[17] investigated the effect of the combination of Ag with La deposited on γ-Al_2O_3. The authors reported full conversion of N_2O at 600°C with 5 wt.%Ag-1 wt.%La_2O_3/γ-Al_2O_3. Konkol *et al.*[48] prepared (34.6 wt.%)Ag/Y_2O_3 via thermal decomposition of a coordination polymer precursor. This material showed 50% conversion at temperatures as high as 400°C.

Silver was also used as a promoter for different mixed metal oxides. E.g. Liu *et al*.[49] studied the effect of Ag doping on some perovskite-type oxides for deN_2O and the reduction of NO. They reported 1 wt.% of Ag as an optimum amount for doping $La_{0.6}Ce_{0.4}CoO_3$. The incorporation of Ag^{1+} altered oxidation state of cobalt, the density of oxygen vacancies and the mobility of lattice oxygen. The silver doped perovskite-type oxides were also successfully prepared and tested in deN_2O by Kumar *et al*.,[50]. The activity of $La_{0.8}Ba_{0.2}MnO_3$ significantly improved by adding 1 wt.% of Ag, especially in

the range of 400-500°C. The presence of silver altered the redox properties of the catalyst, modifying the ratio Mn^{4+}/Mn^{3+} (Fig. 8.).

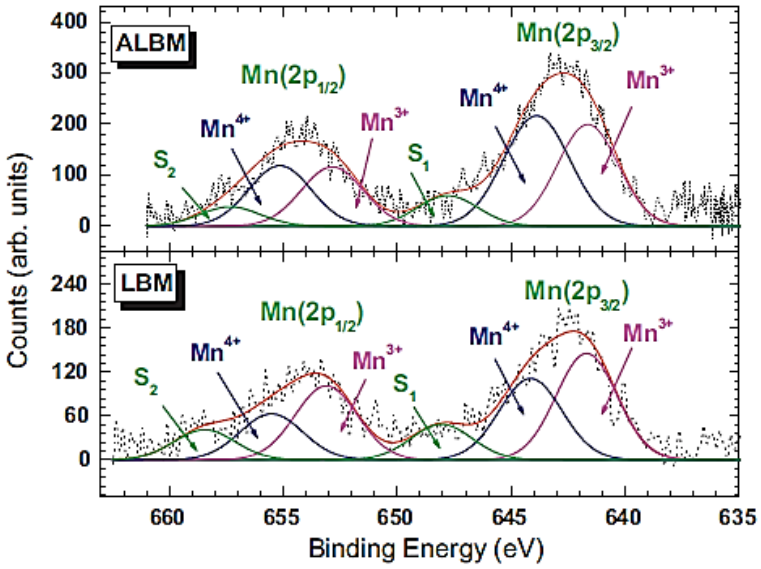

Fig. 8. XPS deconvoluted spectra for Mn2p core level: $La_{0.8}Ba_{0.2}MnO_3$ (LBM) and 1wt.% $Ag/La_{0.8}Ba_{0.2}MnO_3$ (ALBM) (Journal of Molecular Catalysis. A, Chemical 348, 42–54 (2011).

Zhao *et al.*[51] investigated the promotional effect of silver deposition into Co-Al-O_x calcined HT-l compounds and tested it for methane combustion. As evidenced by the H_2-TPR profiles, the deposition of silver modified the redox properties of the catalyst, leading to the formation of more reducible cobalt oxide species (Fig. 9.).

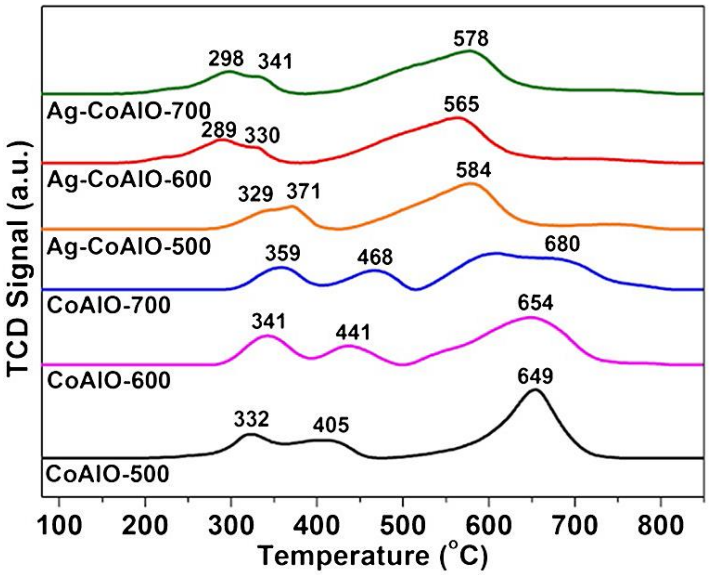

Fig. 9. H_2-TPR plots of calcined Co-Al and Co-Al-Ag HT-l compounds (ChemCatChem 7, 1966–1974 (2015))

These results indicate the possibility to obtain considerable improvements of the catalytic activity of various mixed metal-based catalysts after doping with silver. A small amounts of silver (0.7-1 wt.%) can be easily deposited onto oxide's surfaces or

even incorporated into the oxide structure, altering the physiochemical properties of the potential catalyst with unusual activity.

Several studies reported the enhanced activity of H_2-pretraeted silver-containing materials before deNO_x[52–55], however, there is not a clear explanation about such boosting effect. One of the possible reason refers to formation of $Ag_n^{\delta+}$ clusters after the treatment with H_2.

However, the enhanced activity from the addition of H_2 to the feed cannot be attributed exclusively to the formation of silver clusters, but it has proposed that hydrogen itself participates directly in the reaction mechanism.[56] It has reported that H_2 enhanced the removal of $O_{(ads)}$ molecules on the catalysts' surface: (Eq 6-7)[57,58]

$$H_2 + 2* \rightarrow 2H_{(ads)} \quad (6)$$

$$2H_{(ads)} + O_{(ads)} \rightarrow H_2O + 3 * \quad (7)$$

Kondratenko *et al.*[59,60] showed that the formation of N_2O in NO SCR with NH_3 over Ag/Al_2O_3 significantly decreased in presence of hydrogen, especially for low-temperature operations. H_2 led to the formation of reduced Ag species, which decompose the N_2O produced during the SCR of NO with NH_3. These studies may be helpful not only for the suppression of the N_2O emissions in NH_3-SCR of NO over Ag-containing catalysts but also for deN_2O from exhausts.

1.5 Aim of the thesis

This work is focused on the study of cobalt-based mixed metal oxides, partially modified with silver, for application in deN_2O. The Co(Cu)-(Mg)-Al-O_x or Ag-Co-(Mg)-Al-O_x catalysts were obtained from calcination of hydrotalcite-like precursors. The silver was incorporated during coprecipitation process in order to achieve a close interaction among the metals and yields homogeneously distributed oxides. The specific goals of this thesis are:

- synthesis of Co(Cu)-(Mg)-Al hydrotalcite-like precursors;
- preparation of Co(Cu)-(Mg)-Al-O_x through two synthesis route: (i) thermal decomposition of hydrotalcite-like compounds or (ii) aqueous solution of metal nitrates;
- preparation of Ag-doped catalysts through two modifications route: (i) introduction during coprecipitation or (ii) impregnation with aqueous solution of silver nitrate;

- characterization of the materials applying XRD, TGA, N_2 physisorption, H_2-TPR and XPS;
- N_2O decomposition test in *ideal conditions* (only N_2O/N_2 in the feed) and *real conditions* (in presence of O_2 and/or NO);
- correlation of the activity with the physicochemical properties of catalysts.

Chapter 2: Experimental section

This chapter is divided into three main parts. The first one describes the methods used to prepare precursors and modify their calcined forms. The second part briefly presents the techniques employed for the catalysts' characterization. The final part describes the set-up used to perform catalytic tests of N_2O decomposition.

2.1 Catalysts preparation

The Co(Cu)-(Mg)-Al-O_x catalysts were synthesized by two different routhes:

(i) coprecipitation of hydrotalcite-like precursors, and then it subsequent calcination.

(ii) thermal decomposition of aqueous solution of metal nitrates.

The materials obtained through both syntheses were calcined in static air, at 600°C, for 6 h, with a temperature ramp of 10 °C/min. The materials with molar ratio of Co/Al = 3/1 and Co/Mg/Al = 3/1/1 were selected for further modifications with noble metals (Ag or Rh) by coprecipitation or impregnation. Table 1 summarizes all prepared catalysts.

2.1.1 Coprecipitation

The hydrotalcite-like compounds with intended molar ratio were prepared by coprecipitation, using the following metal nitrates as precursors:

- $Co(NO_3)_2 \cdot 6H_2O$ (Sigma-Aldrich) Purity: ≥98%.
- $Cu(NO_3)_2 \cdot 3H_2O$ (Sigma-Aldrich) Purity: ≥98%.
- $Al(NO_3)_3 \cdot 9H_2O$ (Sigma-Aldrich) Purity: ≥98%.
- $Mg(NO_3)_2 \cdot 6H_2O$ (Sigma-Aldrich) Purity: 99%.

The metal's precursors were dissolved in distilled water, and afterwards the obtained solution was added dropwise and under vigorous stirring, to a solution of Na_2CO_3 (Sigma-Aldrich, purity: ≥98%). During the whole synthesis process the pH was maintained constant at 10±0.2, by adding a 1 M solution of NaOH (Sigma-Aldrich, purity: ≥98%), and the temperature at 60°C. The obtained solution was left under vigorous stirring at 60°C for 0.5 h (Fig. 10). Afterwards it was filtered and washed several times with distilled water,. The obtained solid was dried at room temperature, crushed in a mortar and then calcined (600°C, 6 h, 10°C/min).

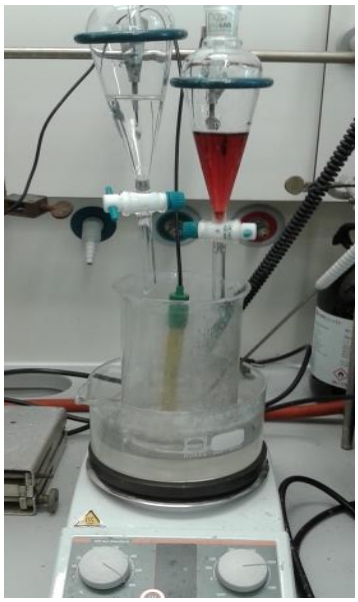

Fig. 10 Synthesis of HT-l compounds by coprecipitation.

2.1.2 Thermal decomposition

The catalysts prepared by thermal decomposition were obtained from aqueous solution of precursors' nitrates dissolved in distilled water, and subsequently dried in the oven at 80°C for 24 h. The obtained solid was crushed in a mortar and calcined (600°C, 6 h, 10°C/min).

2.1.3 Silver-doping

In order to obtain silver-doped catalysts, two different methods were applied:

- coprecipitation: the appropriate amount of an aqueous solution of silver nitrate ($AgNO_3$, Sigma-Aldrich, purity: ≥98%) was added during the HT-l compounds synthesis in order to incorporate silver into the brucite-like structure,
- impregnation: 1 g of the calcined material (600°C, 6 h, 10°C/min) was impregnated with 0.2 M aqueous solution of silver nitrate ($AgNO_3$, Sigma-Aldrich, purity: ≥98%). Subsequently, the Ag-doped solid was dried at room temperature and calcined in static air at 600°C, for 3 h with a temperature ramp of 10°C/min.

2.1.4 Rhodium doping

The procedure for Rh-containing materials were similar, thus, rhodium nitrate ($Rh(NO_3)_3$, Sigma-Aldrich, ~36% rhodium basis) were added during coprecipitation in

order to incorporate the rhodium into the brucite-like structure. The obtained precursor was calcined according to above given calcination procedure.

Table 1 List of prepared catalysts together with their molar ratio. TD: prepared by thermal decomposition, CHT: prepared from calcination of HT-l compounds.

Sample code	**Co_3Al**	**Co_3MgAl**	**Co_2CuAl**	**$Co_{1.5}Cu_{1.5}Al$**	**$CoCu_2Al$**
Molar ratio	Co/Al 3/1	Co/Mg/Al 3/1/1	Co/Cu/Al 2/1/1	Co/Cu/Al 1.5/1.5/1	Co/Cu/Al 1/2/1
CHT	✓	✓	✓	✓	✓
TD	✓	✓	✓	✓	✓
CHT+0.7 wt.% Ag imp.	✓	✓			
CHT+0.7 wt.% Ag cop.	✓	✓			
CHT+0.7 wt.% Rh cop.		✓			
CHT+1 wt.% Ag cop.	✓				
CHT+1.4 wt.% Ag cop.	✓	✓			
CHT+2.1 wt.% Ag cop.	✓	✓			
CHT+2.8 wt.% Ag cop.	✓				

2.2 Catalysts characterization

The catalysts were characterized by the following techniques:

- X-ray diffraction,
- thermogravimetric analysis (TGA),
- N_2 physisorption,
- hydrogen temperature-programmed reduction (H_2-TPR).
- X-ray photoelectron spectroscopy (XPS).

2.2.1 X-Ray Diffraction (XRD)

X-ray powder diffraction (XRD) is a rapid analytical technique primarily used for phase identification of a crystalline material and it can provide information on unit cell dimensions.[61] The interaction between an incident beam of monochromatic X-rays with a target material produces diffracted rays, depending on the distance between planes d and the diffraction angle Θ.[62]

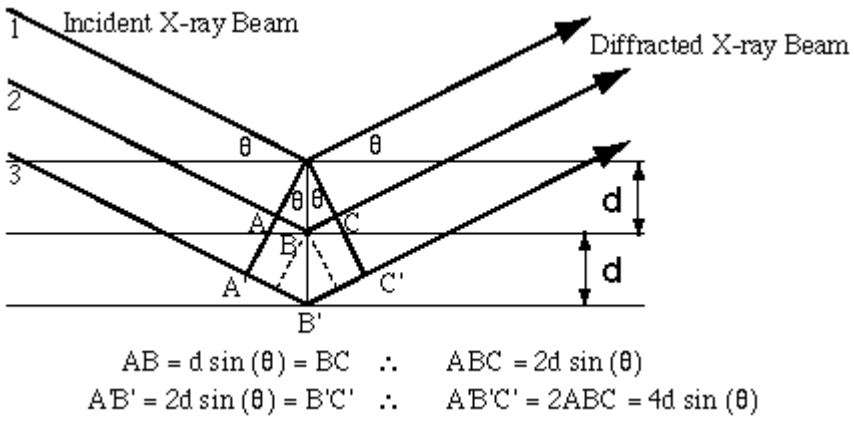

Fig. 11 X-rays diffraction (http://www.chimicamo.org/chimica-generale/diffrazione-dei-raggi-x.html)

The diffracted rays that can overlap and produce constructive or destructive interferences, according to Bragg's law (Eq. 8):

$$n\lambda = 2dsin(\theta) \tag{8}$$

where:

- n - integer number,
- d - distance between crystalline planes,
- λ: wavelength of the incident ray,
- Θ:- diffraction angle.

The interference is at least partially destructive unless the path difference 2dsin(Θ) is equal to an integral number of wavelengths[63]. When an XRD analysis is carried out the diffracted radiation intensity is recorded as function of the incident angle Θ, producing a diffractogram characteristic for every crystal. Mixtures of crystalline materials can also be analysed and the relative peak heights may be used to obtain semi-quantitative estimates of abundances[7].

XRD analysis were carried out using a Siemens D5000 with Cu-Kα radiation (λ = 1.54056Å, 45 kV, 40 mA) in order to investigate the phases present and to determine the lattice parameters of the HT-l precursors. The cell parameters were calculated using a position of (1 1 0) reflection: $a = 2(d_{110})$ and positions of basal reflections: $c = [3(d_{003}) + 6(d_{006})]/2$. The crystal sizes were calculated from the Scherrer equation (Eq. 9):

$$D = \frac{0.89 \cdot \lambda}{\beta \cdot \cos\theta} \tag{9}$$

where:

- D - crystallite size,
- λ: wavelength of the incident ray,
- ß: reflection broadening
- Θ: diffraction angle.

2.2.2 Thermogravimetric analysis (TGA)

Thermogravimetric analysis (TGA) is a thermal method that measures the weight loss of the sample by increasing the temperature, under a controlled atmosphere. It is used to investigate the material's thermal stability, filler content in polymers, and the percent composition of components in a compound. A TGA analysis is performed by gradually raising the temperature of a sample in a furnace as its weight is measured on an analytical balance that remains outside of the furnace. In TGA, mass loss is observed if a thermal event involves loss of a volatile component, like after a combustion process. The results of a thermogravimetric analysis can be expressed in terms of:

- weight loss versus temperature (thermogravimetric curve),
- rate of loss of weight versus temperature (differential thermogravimetric curve).[64]

Thermogravimetric analysis was carried out in order to investigate the thermal transformation of the HT-l precursors. The analysis was carried out using a Netzsch STA 409C/CD, operating under a flow of air (10 cm^3/min) in the temperature range of 30-1000°C with a linear heating rate of 5°C/min.

2.2.3 N_2 physisorption

Gas physisorption is the most common experimental method used for the surface and pore characterization of porous materials, since it allows assessment of a wide range of pore size and it is not that cost intensive compared to some of the other available method. The analysis of surface area and pore volume of the materials were carried out by measuring the absorption isotherm of N_2 at -196°C of the samples using a Quadrasorb^{TM}-evo device (Quantachrome Corporation, Fig. 12).

Fig. 12 Quadrasorb for N_2-Physisorption measurements

Prior to the determination of an isotherm, all samples were outgassed under high vacuum at 200°C with a Quantachrome Flovac degasser. The sample was then placed in a bulb cell kept at –196°C with liquid nitrogen and the analysis was carried out. The specific surface area (S_{BET}) and the total pore volume (V_P) were calculated using the BET model (developed by Brunauer, Emmett and Teller, Eq. 10).[65]

$$\frac{\frac{p}{p0}}{n(1-\frac{p}{p0})} = \frac{1}{nmC} + \frac{(C-1)p}{nmCp0} \quad (10)$$

with p/p_0 in the range of 0.05-0.3; where:

- p - pressure,
- p_0: saturation pressure,
- n: number of moles adsorbed,
- n_m: number of moles adsorbed in the monolayer,
- C: BET constant, relative to the heat of absorption.

By plotting $\frac{\frac{p}{p_0}}{n(1-\frac{p}{p_0})}$ versus $\frac{p}{p_0}$ a linear relationship is obtained and the values of C and n_m can be calculated. From the value of n_m the specific surface areas of the materials was determined by the following equation (Eq. 11):[65]

$$S = nm \cdot am \cdot Na \cdot 10\exp(-21) \quad (11)$$

where:

- S - apparent surface area (m^2/g),
- A_m: area occupied by one adsorbed molecule (m^2/molecule),
- N_a: Avogadro's number (molecules/mol).

2.2.4 Hydrogen temperature-programmed reduction (H_2-TPR)

Temperature-programmed reduction with H_2 (H_2-TPR) is a common technique used to investigate the redox properties of the catalysts. In analysis gas (H_2 in an inert carrier gas such as N_2, Ar or He) flows through the sample, usually at room temperature. While the gas is flowing, the temperature of the sample is increased linearly with time and the consumption of H_2 by reduction processes of transition metal oxides is monitored. The obtained H_2-TPR profile is a plot of the amount of hydrogen consumed versus the temperature.[66]

The H_2-TPR analysis was carried out using a ChemBET Pulsar TPR/TPD device (Quantachrome Corporation, Fig. 13). Prior to the analysis, 30 mg of the sample was pretreated using an Ar flow of 20 cm^3/min, with a temperature ramp of 25°/min until 600°C. Then the sample was treated with a flow of 5.0 vol.% of H_2 in Ar (25 cm^3/min), and heated up from room temperature to 1000°C with a heating rate of 10°C/min. The hydrogen consumption was detected by a thermal conductivity detector, while the water generated during the measurement was removed by a cold trap, placed before the detector.

Fig. 13. ChemBet Pulsar for H_2-TPR measurements.

2.2.5 X-ray photoelectron spectroscopy (XPS)

X-ray photoelectron spectroscopy is a surface spectroscopy technique that involves the irradiation of the sample in vacuum with monoenergetic soft x-rays (Mg K_α X-rays or Al K_α X-rays are ordinarily used) and sorting the emitted electrons by energy. The photons of the incident X-ray beam are low penetrating, so they interact only with the atoms on the surface of materials, causing the emission of electrons by photoelectron effect (Fig. 14).

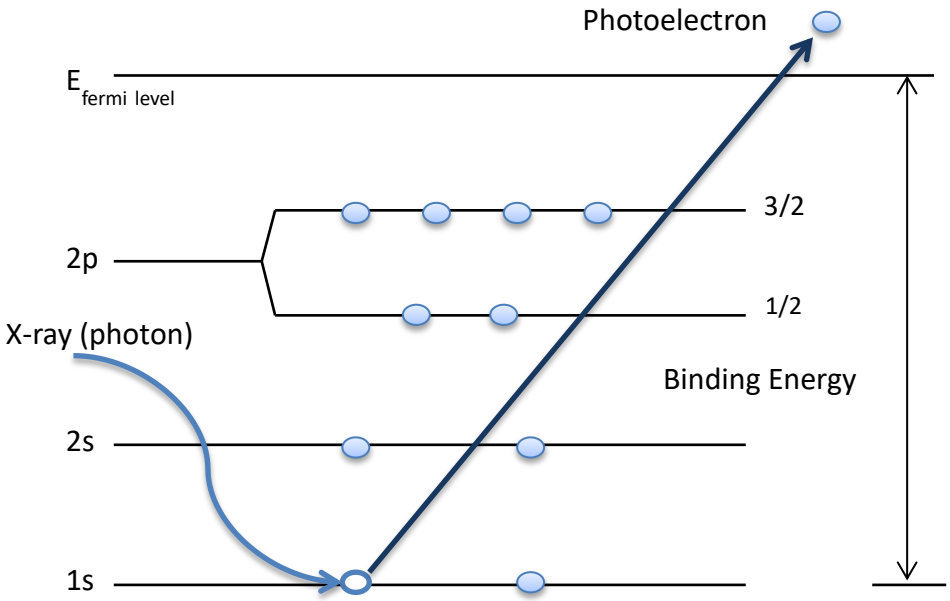

Fig. 14 Photoelectric effect (https://fas.dsi.a-star.edu.sg/equipments/xps_10.aspx)

The electrons leaving the sample are detected by an electron spectrometer, according to their kinetic energy (Eq. 12):

$$Ek = h\nu - BE - \Phi s \tag{12}$$

where:

- E_k - kinetic energy of the emitted electron;
- hν: energy of the photon;
- BE: binding energy of the orbital from which the electron originates;
- Φ_s: spectrometer work function.

The obtained spectrum (unique for each element) is a plot of the number of emitted electrons for energy interval, versus their binding energy, determined by the previous equation. From XPS analysis is then possible to obtain information regarding the oxidation state, the electronic structure and the atomic composition of the sample's surface. [67]

X-ray photoelectron spectra were measured on a VSW spectrometer equipped with a hemispherical analyzer. The photoelectron spectra were measured using a magnesium MgKα source (E = 1253.6eV). The base pressure in the analysis chamber during the measurements was $3 \cdot 10^{-6}$ Pa and the spectra were calibrated on a main carbon C1s peak at 284.6 eV. Mathematical analyses of the XPS spectra were carried out using the XPSpeak4.1 computer software (RWM. Kwok, The Chinese University of Hong Kong).

XPS analysis was carried out in order to obtain information regarding the s the oxidation state and the atomic ratio of cobalt to silver.

2.3 Catalytic tests

Catalytic N_2O decomposition tests were carried out in a quartz fixed bed reactor under atmospheric pressure, using 350 mg of calcined catalyst (grain dimensions selected between 250 and 500 µm), and the effluent gases of the reactor were analysed by an IR spectrometer. Prior to the catalytic tests the catalysts were pretreated with a N_2 flow of 100 cm^3/min, raising the temperature from 50 to 600°C, with a temperature ramp of 10°C/min, and then cooling to 50°C. During the catalytic tests the temperature of the reactor was raised from 50 to 600°C or until full N_2O conversion, using 50°C steps. Each temperature was set constant for 30 min before recording an IR spectrum. Fig. 15 presents the set-up diagram i.

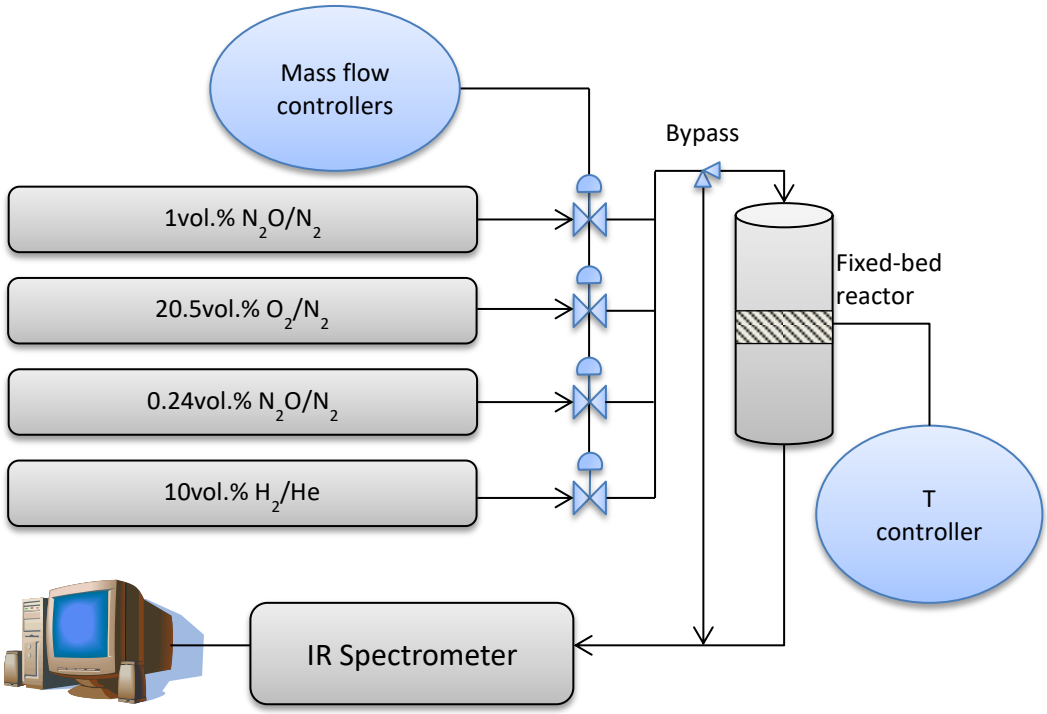

Fig. 15 Set-up diagram

The catalytic tests were carried out in two different reaction conditions:

- *ideal conditions* with 0.1 vol.% N_2O diluted in N_2;
- *real conditions* with 0.1 vol.% N_2O, 4.5 vol.% O_2, 0.03 vol.% NO diluted in N_2.

The contact time $M_{catalyst}/ \dot{V}_{feed}$ was 0.0583 $g \cdot h \cdot L^{-1}$

For the most active catalysts (1 wt.% Ag/CHT-Co_3Al) an additional stability test was performed at 400°C for 30 h under *real conditions*. An IR spectrum was collected every 1 h.

Furthermore, for a selected group of materials, catalytic tests were carried out using an H_2-pretreatment. Thus, before reaction the catalyst was heated up from 50 to 600°C, using a flow of 5.0 vol.% H_2 diluted in Ar with a flow rate of 100 cm^3/min. Subsequently the material was cooled down in pure N_2. The catalytic test was carried out under *ideal condition*s.

The N_2O conversion was calculated for every temperature step in order to investigate the performances of the catalyst. The calculations were done using the areas of the characteristic peak related to the N_2O stretching at 1298 cm^{-1} (peak 4), since there is a linear correlation between peaks areas and N_2O (Fig. 16).

The conversion was then calculated (Eq. 13)through the following equation:

$$X = \frac{Cin - Cout}{Cin} \cdot 100 \qquad (13)$$

where:

- X - N_2O conversion;
- C_{in}: .N_2O concentration at the inlet of the reactor;
- C_{out}: N_2O concentration at the outlet of the reactor.

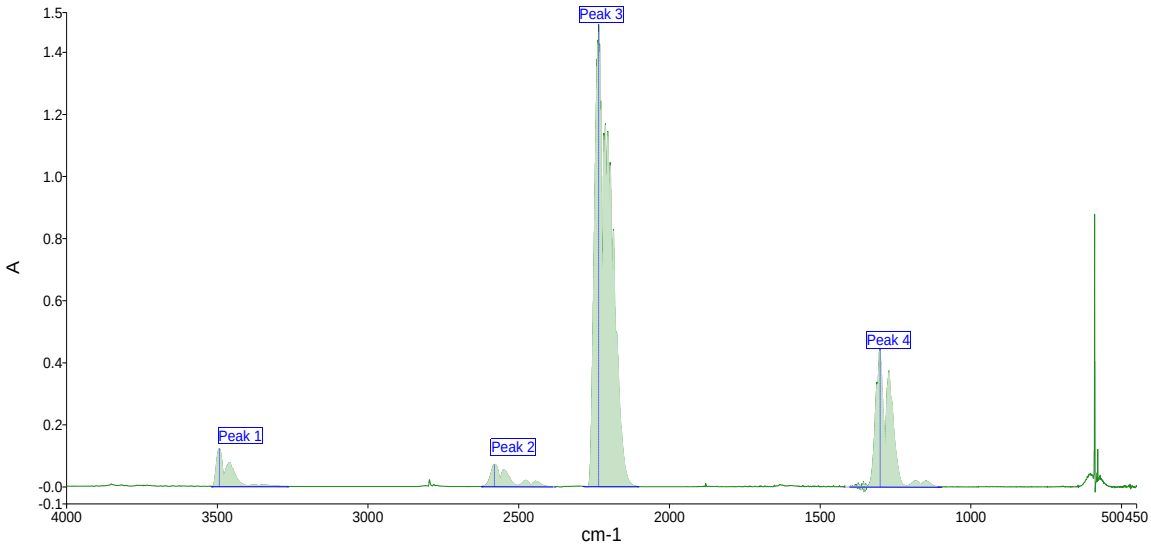

Fig. 16 IR spectrum of N_2O

Chapter 3: Results and discussion

This chapter contains the interpretation of the obtained results. The first part focus on the physicochemical characterization of the catalysts, while the second one concerns the catalytic N_2O decomposition tests.

3.1 Catalysts characterization

The catalysts were characterized by the techniques described in the Chapter 2.2. The first part presents the results obtained from XRD, N_2-physisorption and TGA, which provide information regarding the structural, textural properties as well as thermal stability of the materials. The second part concerns the H_2-TPR and XPS analysis, related to the redox properties and the oxidation state of transition metal of the catalysts.

3.1.1 XRD, TGA and N_2 physisorption

The crystal structure of the materials (before and after calcination) were investigated by X-ray diffraction (XRD). Figures 17-19 presents the XRD patterns of the hydrotalcite-like precursors.

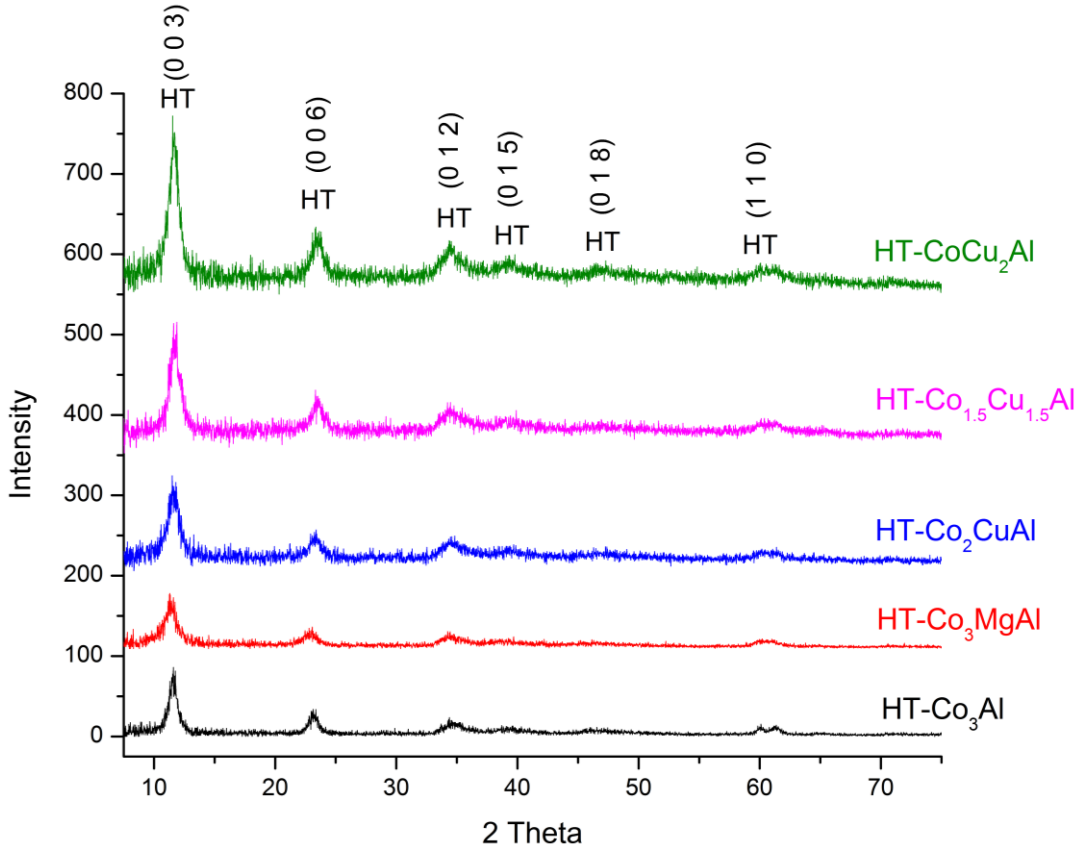

Fig. 17 XRD patterns of HT-l compounds

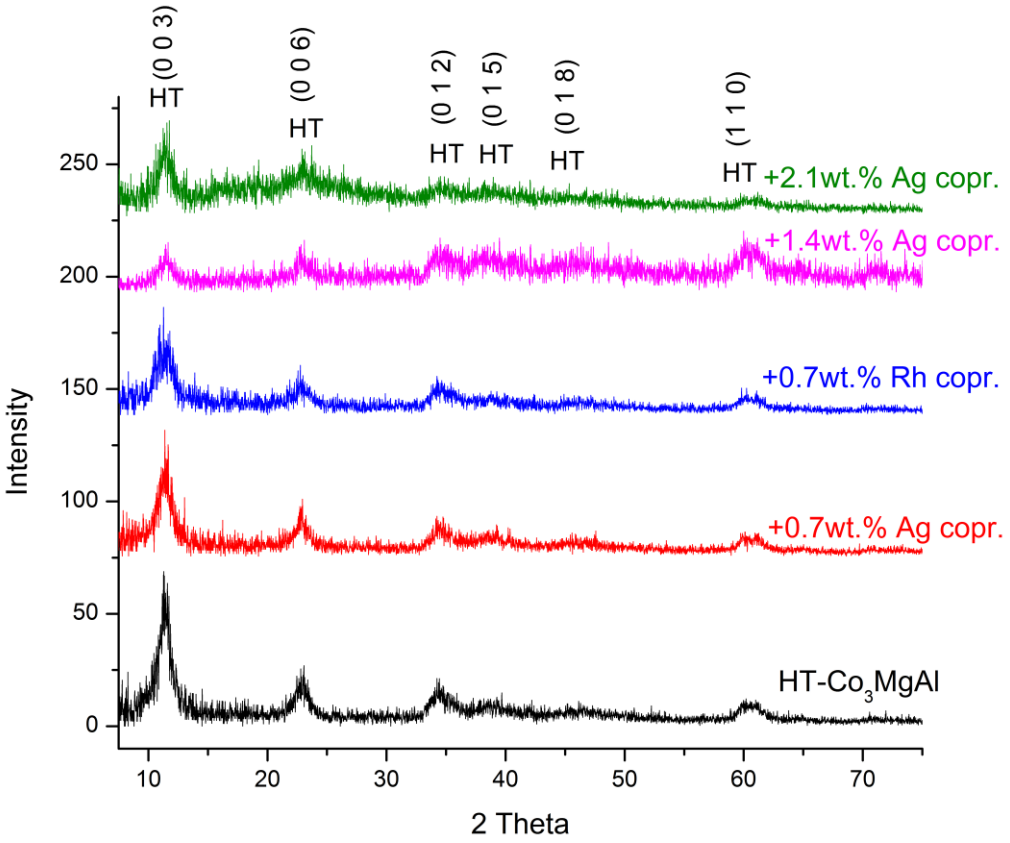

Fig. 18 XRD patterns of Co-Mg-Al HT-l compounds doped with silver

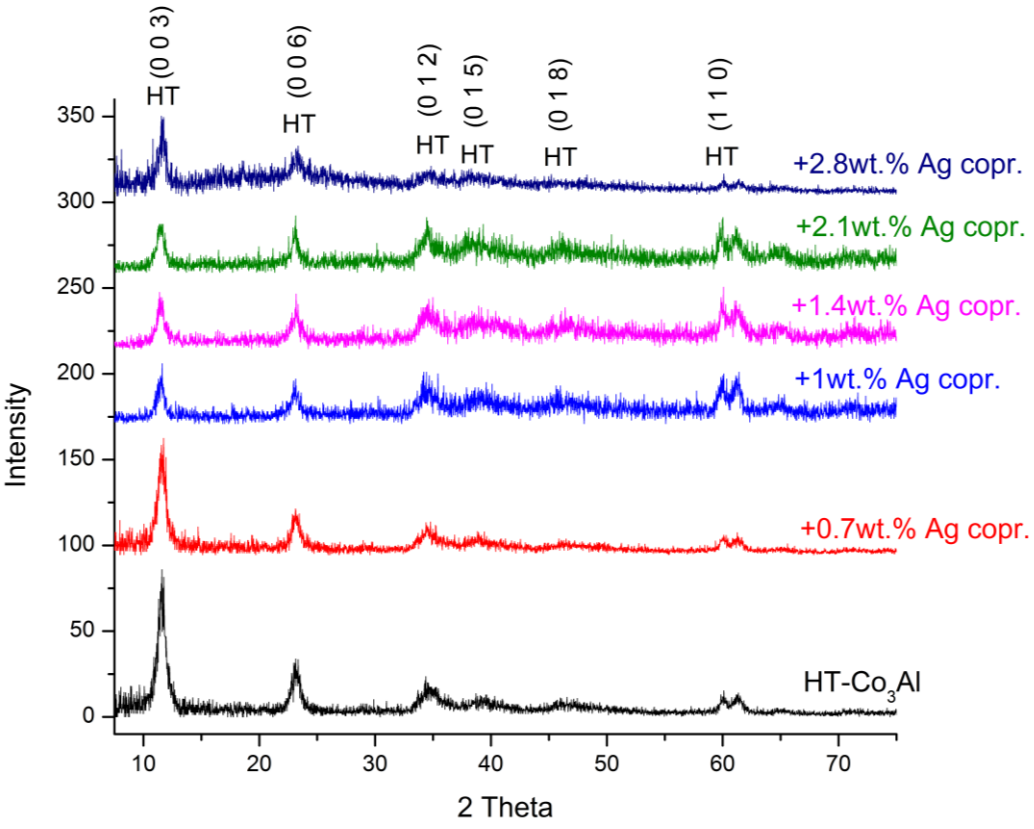

Fig. 19 XRD patterns of Co-Al HT-l compounds doped with silver

All the compounds showed the typical reflections of hydrotalcite-like compounds with reflections at (0 0 3), (0 0 6), (0 1 2), (0 1 5), (0 1 8), and (1 1 0).[19,68,69] The crystallinity of the samples decreased by increasing the amount of silver. The modification with silver led to HT phases reflections progressively broader and less intensive. Table 2 summarizes the cell parameters *a* and *c*, and the crystal sizes (D*c* and D*a*) of the HT-l precursors.

Table 2 Unit cell parameter (*a* and *c*) and crystal dimensions (Dc and Da) of the HT-l precursors

Catalysts code	***c*** **(Å)**	***a*** **(Å)**	**D*c*** **(nm)**	**D*a*** **(nm)**
HT-Co_3Al	22.97	3.079	19	29.1
HT-Co_3Al + 0.7 wt.% Ag copr.	22.95	3.079	20	28.9
HT-Co_3Al + 1 wt.% Ag copr.	23.09	3.084	21.9	31
HT-Co_3Al + 1.4 wt.% Ag copr.	23.04	3.082	20.5	35.3
HT-Co_3Al + 2.1 wt.% Ag copr.	23.1	3.086	25.6	41
HT-Co_3MgAl	23.33	3.085	12.9	20.5
HT-Co3MgAl + 0.7 wt.% Ag copr.	23.33	3.084	13.3	22.9
HT-Co_3MgAl + 0.7 wt.% Rh copr.	23.4	3.079	9.5	13.2
HT-Co_3MgAl + 1.4 wt.% Ag copr.	23.19	3.079	12.3	19.8
HT-Co_3MgAl + 2.1 wt.% Ag copr.	23.2	3.077	11.6	18.1
HT-Co_2CuAl	22.87	3.077	15	13.6
HT-$Co_{1.5}Cu_{1,5}Al$	22.66	3.073	15.8	13.7
HT-$CoCu_2Al$	22.73	3.077	15.9	11.6

The values of the lattice parameters *a* around 3.08 Å and *c* around 23 Å were in good agreement with literature for HT-l compounds with CO_3^{2-} as interlayer anion.[19] The value of *a* is related to the average cation-cation distance in the brucite-like sheets and depends on the ionic radius of the cations in octahedral coordination. The partial substitution of Co^{2+} with Cu^{2+} in the HT-l compounds did not lead to a significant change of *a*, due to their similar ionic radius (0.0745 nm and 0.073 nm, respectively). On the other hand, the introduction of Mg^{2+} (0.072 nm), caused a slight increase of *a*, because its bigger ionic radius compared to Al^{3+} (0.0535 nm). [70]

The parameter *c* is related to the thickness of the interlayer space and depends on the layer-charge density, the nature of the interlayer anion, and the number of water molecules in the interlayer space[19]. Therefore the interlayer distance should increase by

decreasing the electronegativity of the cations in the brucite-like sheets:[71] Cu (1.75) > Co (1.70) > Ag (1.42) > Mg (1.23), according to Allred and Rochow electronegativity scale.[72] Accordingly, Mg-modified samples showed higher values of *c*, compared to Co-Al-O_x. Oppositely, the partial replacement of cobalt with copper caused a slight decrease of the parameter *c*. However, it has to be taken into account that also the interlayer water amount influences this parameter.[71]

The incorporation of small quantity of silver in the HT-l structure caused a distortion of the crystal structure, as evidenced by XRD patterns. Both lattice parameters *a* and *c* increased after the introduction of silver up to 1 wt.%.

Table 3 summarizes the specific surface areas (S_{BET}) and total pore volumes (V_p) of the calcined samples.

Table 3 Specific surface areas (S_{BET}) and total pore volumes (V_p) of the calcined samples

Catalysts code	S_{BET} (m^2/g)	Pore volume (cm^3/g)
CHT-Co_3Al	81.6	0.456
TD-Co_3Al	28.9	0.196
CHT-Co_3Al + 0.7 wt.% Ag impr.	61.1	0.379
CHT-Co_3Al + 0.7 wt.% Ag copr.	66.4	0.387
CHT-Co_3Al + 1 wt.% Ag copr.	67.8	0.411
CHT-Co_3Al + 1.4wt.% Ag copr.	70.5	0.423
CHT-Co_3Al + 2.1wt.% Ag copr.	62.1	0.392
CHT-Co_3Al + 2.8wt.% Ag copr.	53.0	0.369
CHT-Co_3MgAl	47.7	0.271
TD-Co_3MgAl	28.2	0.097
CHT-Co_3MgAl + 0.7wt.% Ag impr.	41.2	0.251
CHT-Co_3MgAl + 0.7wt.% Ag copr.	42.2	0.323
CHT-Co_3MgAl + 0.7wt.% Rh copr.	48.2	0.218
CHT-Co_3MgAl + 1.4wt.% Ag copr.	51.9	0.242
CHT-Co_3MgAl + 2.1wt.% Ag copr.	45.1	0.427
CHT-Co_2CuAl	57.1	0.372
TDCo_2CuAl	30.4	0.125
CHT-$Co_{1.5}Cu_{1.5}Al$	59.2	0.362
TD$Co_{1.5}Cu_{1.5}Al$	28.8	0.140
CHT-$CoCu_2Al$	62.8	0.486
TD$CoCu_2Al$	38.1	0.103

The samples showed specific surface area in the range of 28-82 m^2/g. The hydrotalcite derived mixed metal oxides showed specific surface areas around 2/3 times higher than analogous materials synthesized by thermal decomposition. This effect could be related to the formation of well-crystallized cobalt spinels, characterized by low specific surface areas.[23] Furthermore, Reichle *et al.*[73] reported that the calcination of Co-HT-l compounds led to the generation of pores on the surface of the material through which water molecules and CO_2 were removed from the layered structure. This contributed to the formation of slightly amorphous cobalt spinels with high surface area.

Figure 20 shows the XRD patterns of the calcined catalysts prepared from hydrotalcite-like compounds (CHT) and thermal decomposition (TD).

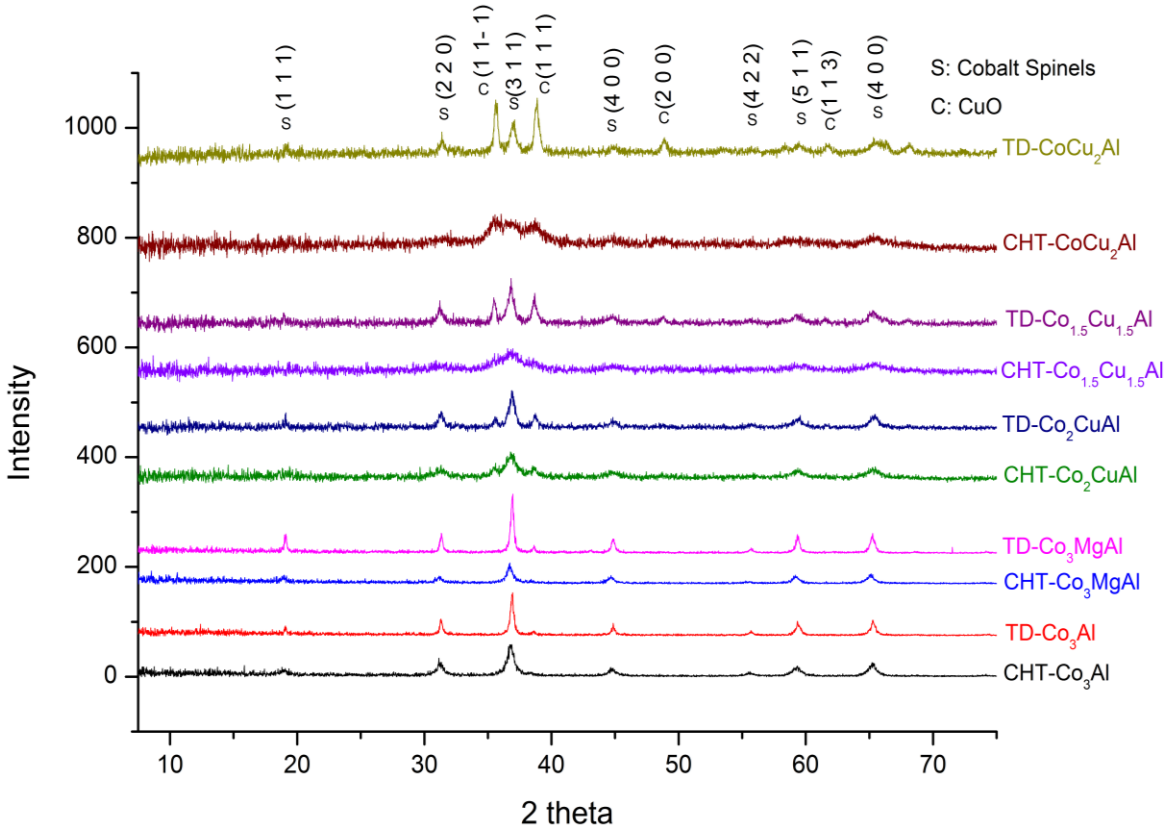

Fig. 20 XRD patterns of Co-Mg-Cu-Al non-doped catalysts

The calcination of the precursors resulted in the disappearance of diffraction lines typical of the HT-l structure and formation of the characteristic reflection of the cobalt spinels, corresponding to the (1 1 1), (2 2 0), (3 1 1), (4 0 0), (4 2 2), and (5 1 1) planes. The different indistinguishable spinel phases, such as Co_3O_4, $CoAl_2O_4$, $MgCo_2O_4$, appeared at similar positions.[23,27,30] The incorporation of copper led to formation of cobalt spinels phases, copper oxide (CuO), whose intensities increase by increasing the amount of copper in the catalysts, and also possibly mixed copper-cobalt spinels

($Cu_xCo_{3-x}O_4$). [24,74–76] The catalysts synthesized by thermal decomposition showed similar phase composition, but higher crystallinity compared to hydrotalcite-derived mixed metal oxides. Figures 21-22 show the XRD patterns of the Ag or Rh-doped catalysts.

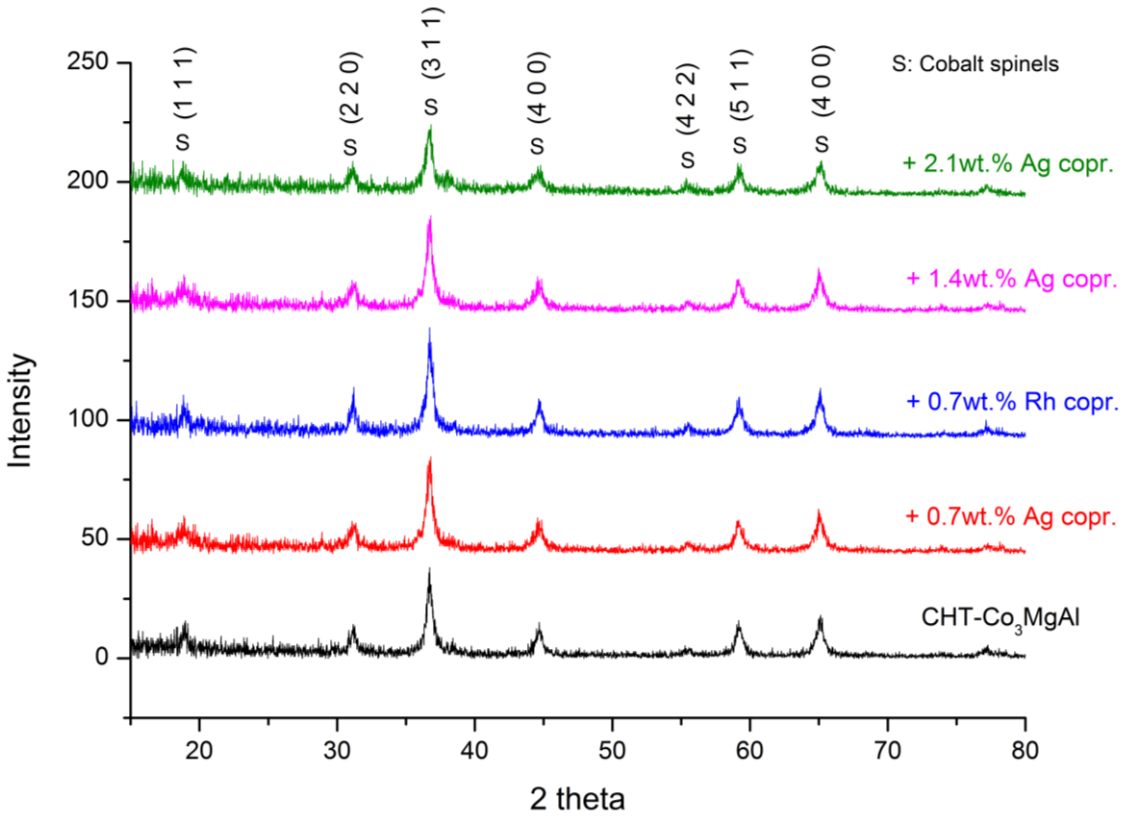

Fig. 21 XRD patterns of Co-Mg-Al calcined HT-l compounds doped with silver

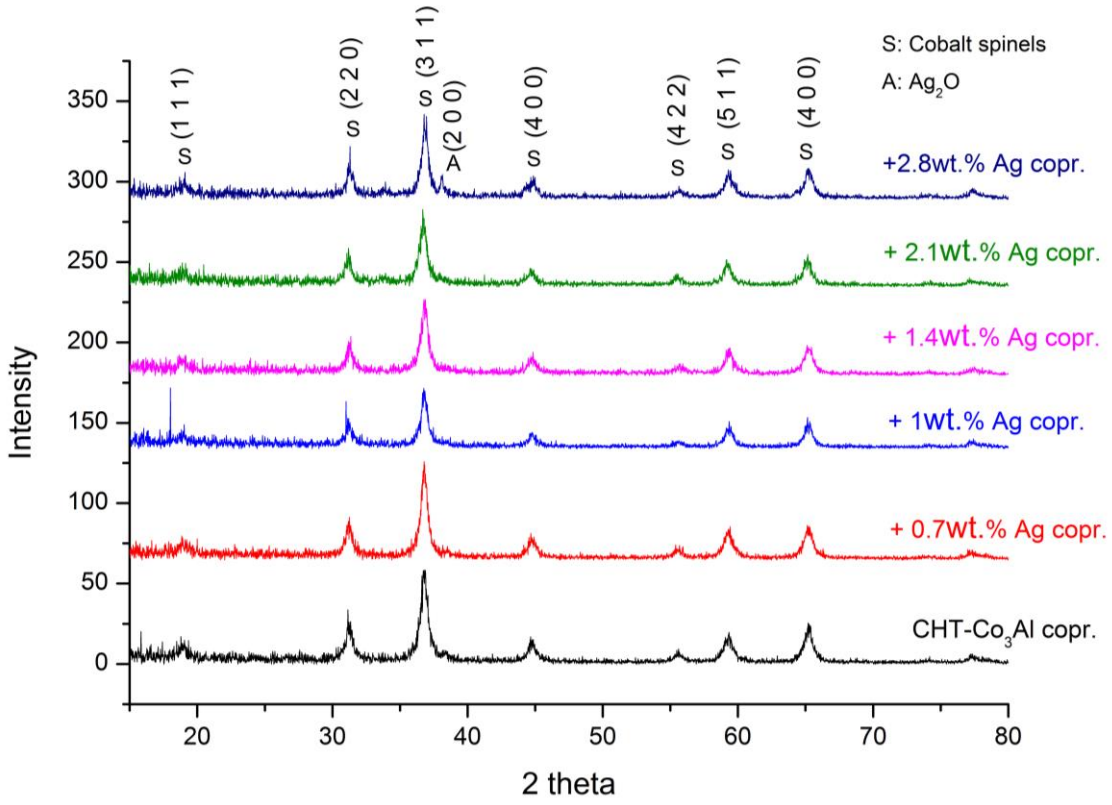

Fig. 22 XRD patterns of Co-Al calcined HT-l compounds doped with silver

Neither noble metal phase nor their oxides were identified in these catalysts. An exception was the sample containing 2.8 wt.% of Ag: the XRD pattern of (2.8wt.% Ag) CHT-Co_3Al shows the characteristic reflection of Ag_2O, suggesting that a separate Ag_2O phase emerges at higher amount of silver incorporation.[50,77,78]

The thermal transformation of the hydrotalcite-like compounds was also investigated by TG-DTG analysis (Fig. 26).

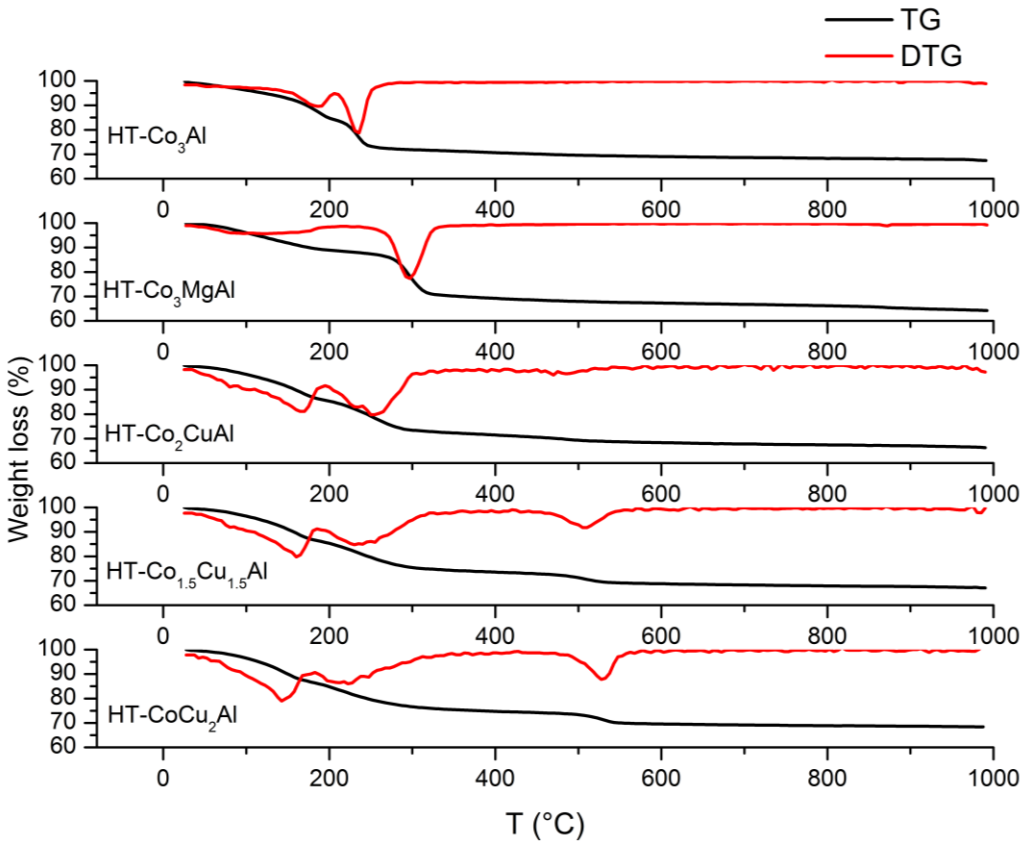

Fig. 23 TGA and DTGA of HT-l compounds

The thermograms show the presence of two endothermic transitions:

(i) below 200°C: associated with the removal of the interlayer and weakly adsorbed water molecules,

(ii) in the range 200-300°C: due to the decomposition of hydroxyl groups and interlayer anions.[19,27,31]

For the Cu-containing catalysts an additional endothermic process appeared around 530°C, which was related to the thermal decomposition of strongly stabilized structural CO_3^{2-}. According to Chmielaraz *et al.*, copper introduced into the HT-l structure stabilized CO_3^{2-} anions, and thus they decomposed at higher temperature [24,79]. Similar thermograms were obtained for Ag- or Rh-doped catalysts (Fig. 27, 28).

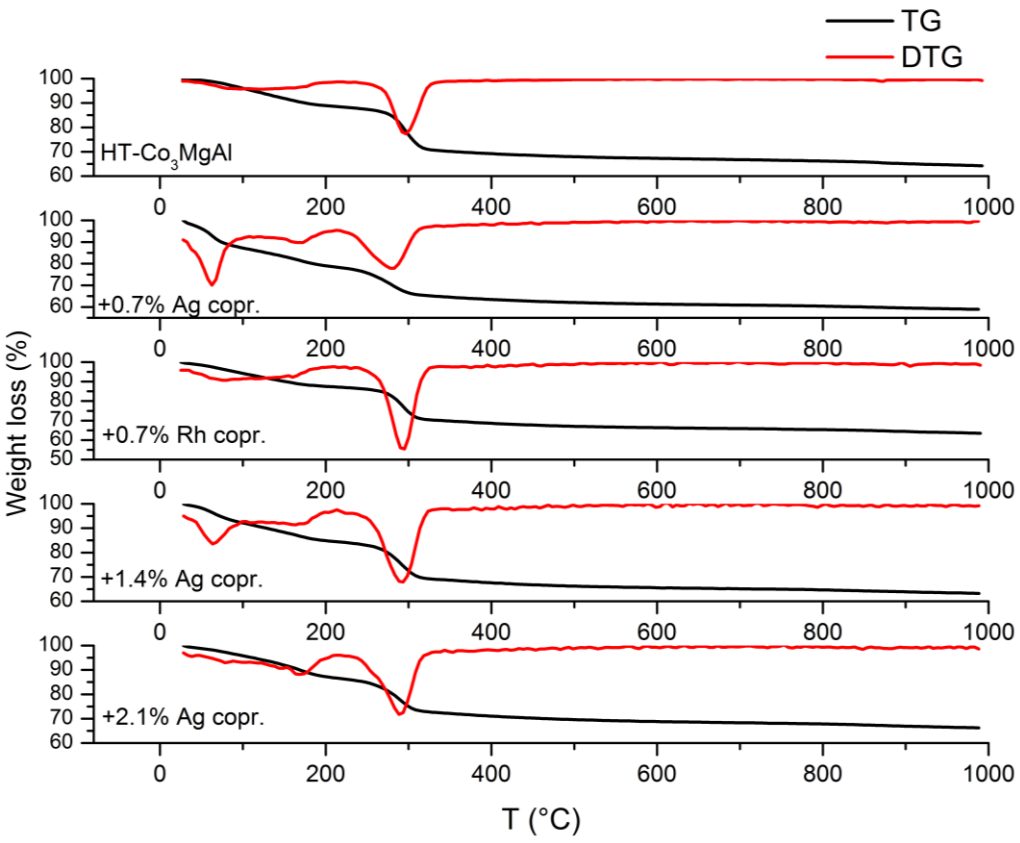

Fig. 24 TGA and DTGA of Co-Mg-Al HT-l compounds doped with silver

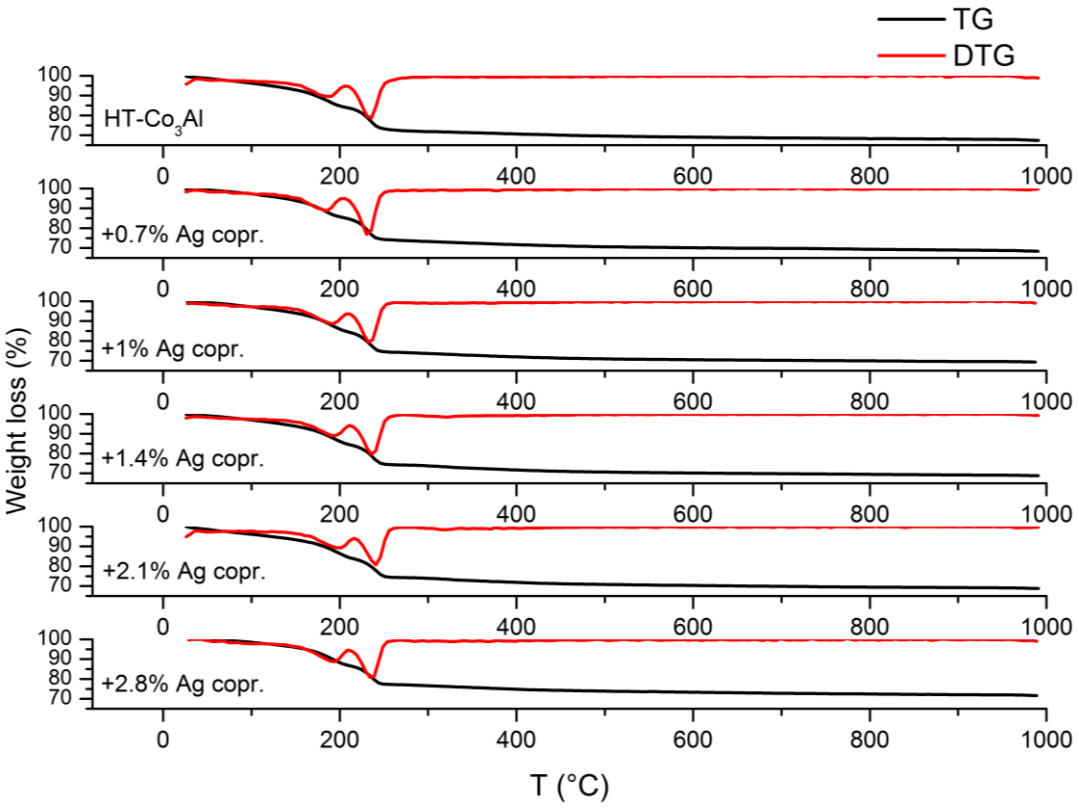

Fig. 25 TGA and DTGA of Co-Al HT-l compounds doped with silver

3.1.2 H_2-TPR and XPS

The redox properties of the catalysts were investigated by temperature-programmed reduction with hydrogen (H_2-TPR) analysis. Figure 26. summarizes the H_2-TPR profiles for the Co(Cu)-(Mg)-Al-O_x hydrotalcite-derived mixed metal oxides.

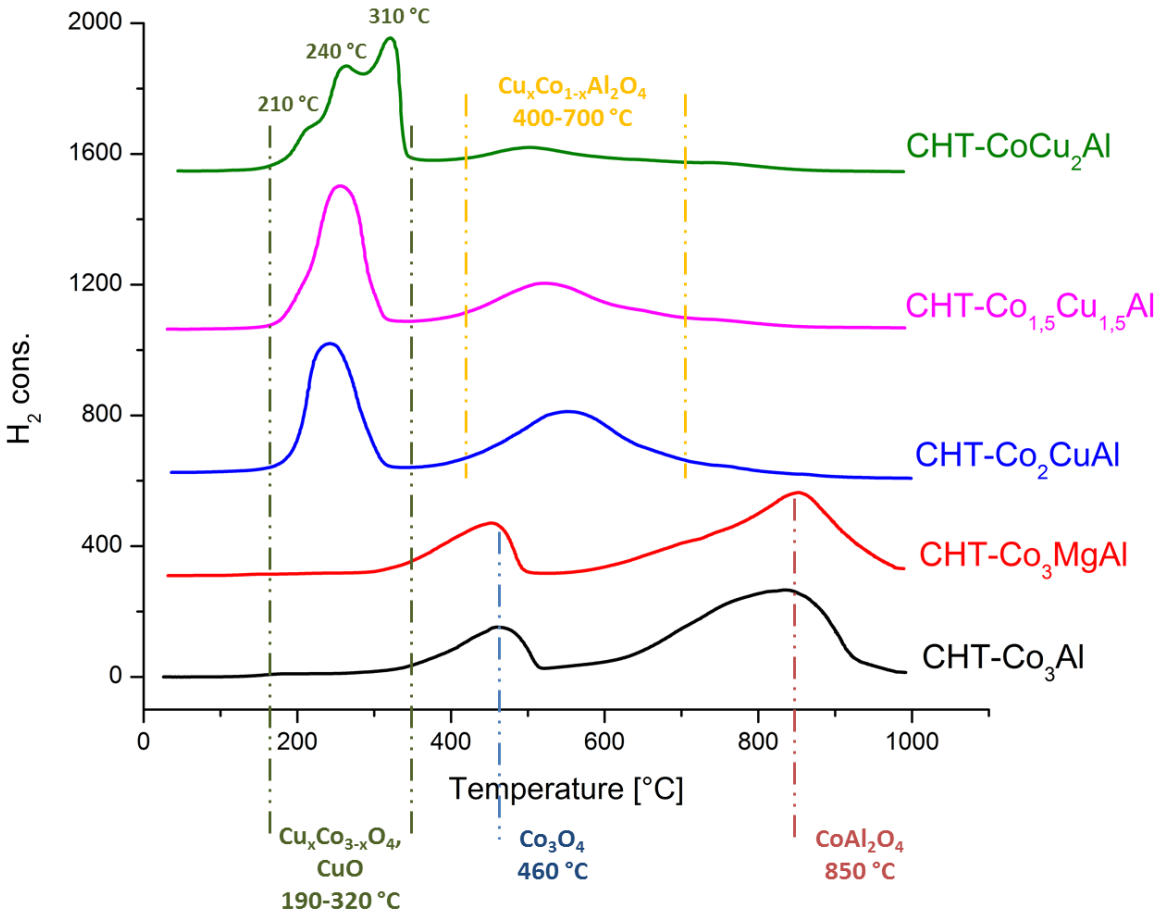

Fig. 26 H_2-TPR profiles of calcined HT-l compounds

The catalysts with compositions Co/Al = 3/1 and Co/Mg/Al = 3/1/1 showed two main reduction peaks at around 450°C and 850°C. The first one appeared due to reduction of Co_3O_4. Since in Co_3O_4 the cobalt is present in mixture of Co^{2+} and Co^{3+}, two reduction peaks should appears (Eq. 14-15):[25,26,36]

$$Co_3O_4 + H_2 \rightarrow 3CoO + H_2O \quad (14)$$

$$CoO + H_2 \rightarrow Co^0 + H_2O \quad (15)$$

Such reduction stages were indiscernible, in the H_2-TPR profile of both Co(Cu)-Al-O_x and Co-Mg-Al-O_x, thus only a broad reduction peak of Co^{3+} to Co^0 appeared at 450°C. The high temperature reduction peak centred at 850°C was related to the reduction of cobalt in $CoAl_2O_4$ (Eq. 16).

$$CoAl_2O_4 + H_2 \rightarrow Co^0 + Al_2O_3 + H_2O \quad (16)$$

The presence of Al influenced the reducibility of the cobalt spinels, thus the reduction peaks shifted to higher temperature.[26,30,80] Arnoldy *et al.* claimed that Al^{3+} polarized the covalent Co-O bonds, increasing the charge of Co^{2+}. Consequently, the lattice energy increased, resulting in higher reduction temperatures of cobalt spinels in both Co-Al-O_x and Co-Mg-Al-O_x.[80] For the material with molar composition Co/Mg/Al = 3/1/1, the formation of $MgCo_2O_4$ cannot be excluded. Cobalt in such spinel is reduced at around 690°C with the following steps (Eq. 17-18):[26]

$$MgCo_2O_4 + H_2 \rightarrow MgCo_2O_3 + H_2O \quad (17)$$

$$MgCo_2O_3 + 2H_2 \rightarrow 2Co^0 + MgO + 2H_2O \quad (18)$$

In the H_2-TPR profiles of the catalysts with molar compositions of Co/Cu/Al = 2/1/1 and 1.5/1.5/1, a single peak appeared at around 250°C, probably related to the reduction of copper in CuO (evidenced by XRD analysis, Fig. 20), and also possibly in $Cu_xCo_{3-x}O_4$ [25,75]. In the H_2-TPR profiles of catalysts with the highest amount of copper (Co/Cu/Al = 2/1/1 mol.%) the peak at lower temperature split into several peaks, due to the reduction of copper and cobalt in the various species , including: CuO, $Cu_xCo_{3-x}O_4$. The peak at 310°C was probably related to the reduction of cobalt in $Cu_xCo_{3-x}O_4$, while the peaks at 210°C and 240°C and to the reduction of copper in CuO and the spinels, respectively.[25,26,75,81] The peaks at higher temperature (maxima between 540 and 600°C) appeared probably due to the reduction of cobalt in $CoAl_2O_4$. However, these peaks were shifted of 200-300°C compared to the ones of the copper-free catalysts. Therefore, the presence of mixed non-stoichiometric spinels $Cu_xCo_{1-x}Al_2O_4$, where copper increased the reducibility of cobalt, cannot be excluded. Moreover, increasing the amount of copper in the materials, the high temperature peak was progressively less intensive, thus the amount of mixed spinels $Cu_xCo_{1-x}Al_2O_4$ gradually decreased.

Figure 27 presents the H_2-TPR profiles of catalysts obtained by thermal decomposition.

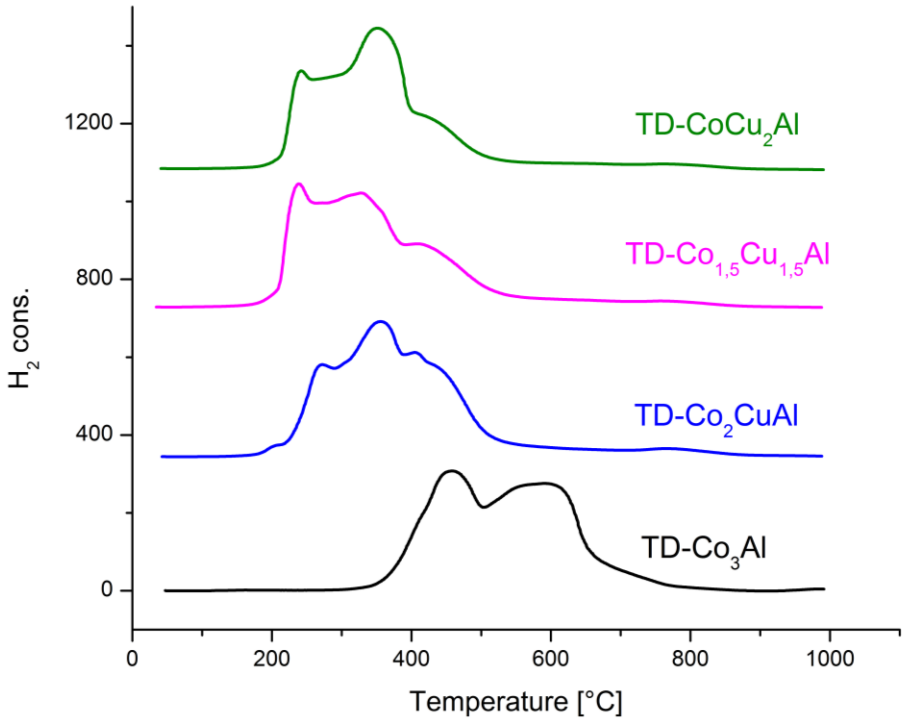

Fig. 27 H_2-TPR profiles of mixed metal oxides prepared by thermal decomposition

The reduction peaks of copper and/or cobalt oxide species were partially overlapped, thus adequate identification of reduction of those species could be speculative.

Figure 28 summarizes the H_2-TPR profiles for Co-Mg-Al-Ox doped with different amounts of Ag or Rh (0.7-2.1 wt.%).

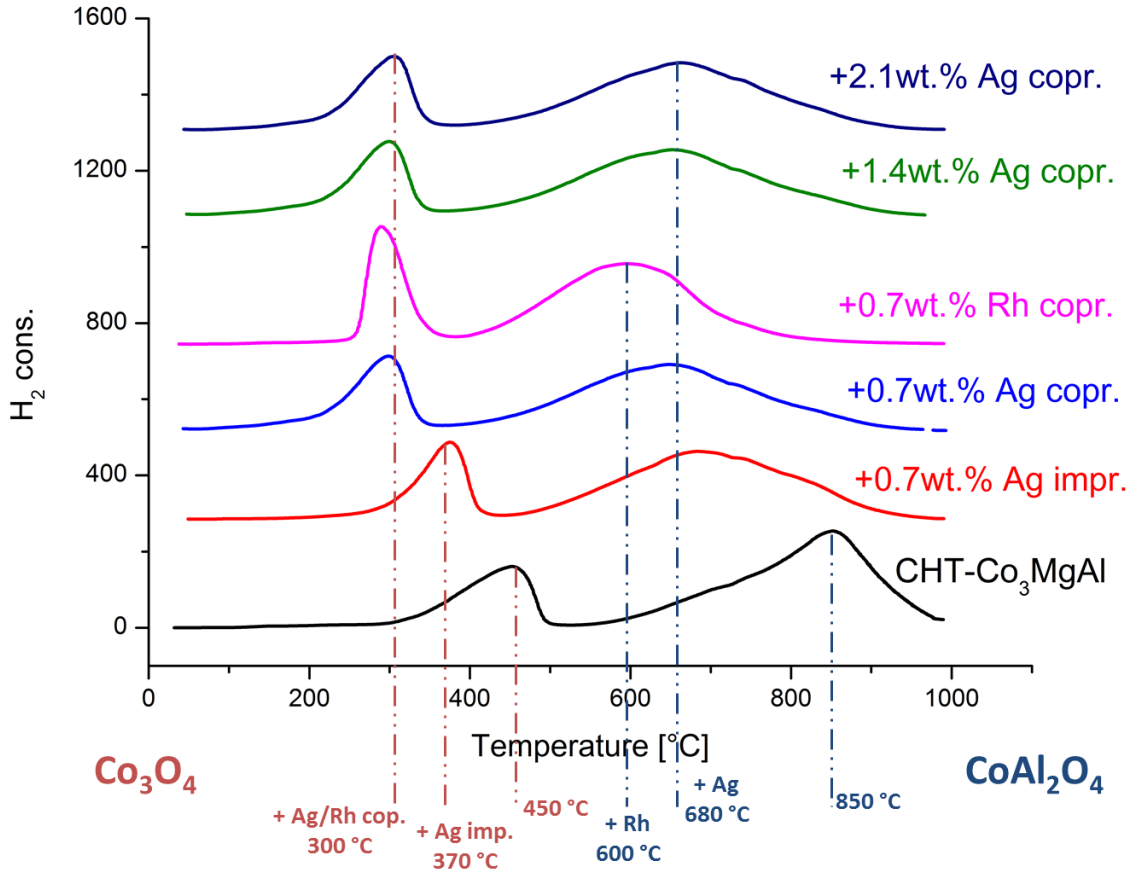

Fig. 28 H_2-TPR profiles of Co-Mg-Al calcined HT-l compounds doped with silver or rhodium

Similarly to the undoped Co-Mg-Al-O_x, the H_2-TPR profiles for Ag- or Rh-modified materials revealed two main peaks, that were related to the reduction of cobalt present in Co_3O_4, $CoAl_2O_4$, respectively.[25,26,30,36,80] Generally, the modification with Ag or Rh influenced the redox properties of the materials, by shifting the reduction peaks to lower temperatures. Thus, the presence of silver oxides species facilitated the reduction of Co^{3+} and Co^{2+} to metallic cobalt. Zhao et al. and Kumar et al.[50,51] evidenced similar results for Ag-doped Co-Al-O_x calcined HT-l compounds and Ag-doped $La_{0.8}Ba_{0.2}MnO_3$, respectively.

For materials with silver above 0.7 wt.%, no further alteration appeared in the H_2-TPR profiles. Presumably because bulk silver oxide segregated during the calcination step, but the concentration of Ag_2O was still too low to produce a noticeable peak in the profile. The H_2-TPR reduction profile varied also depending on the modification methods. E.g. the material with 0.7 wt.% of silver added during coprecipitation showed the reduction temperature of Co_3O_4 lower by about 70°C, than the respective materiel doped through impregnation. Thus, possibly a better dispersion of silver oxide species inside hydrotalcite derived mixed metal oxides was obtained during coprecipitation. The

lowest reduction temperatures with maximum centred about 290 and 600°C, were reached by the sample modified with rhodium. Therefore, the doping with rhodium influenced the redox properties of the materials more significantly than in case of the modification with silver.

Figure 29 summarizes the H_2-TPR profiles for Co-Al-O_x doped with different amounts of Ag (0.7-2.8 wt.%)

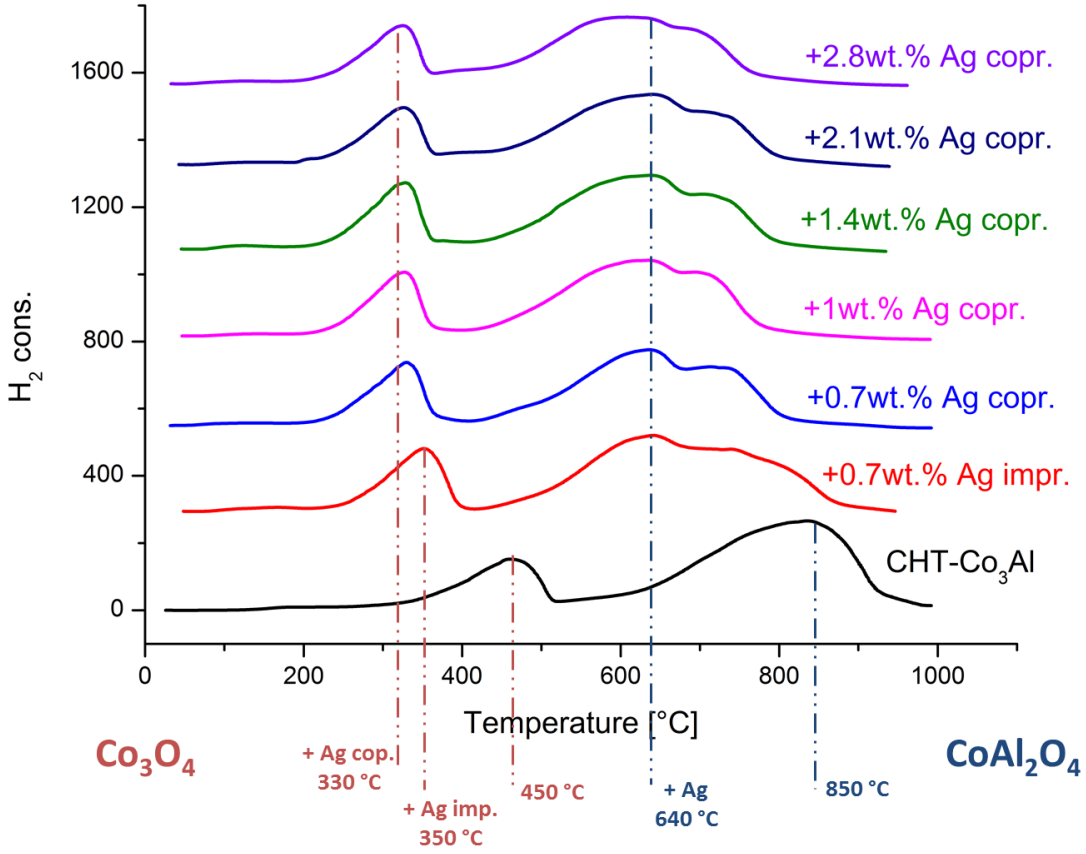

Fig. 29 H_2-TPR profiles of Co-Al calcined HT-l compounds doped with silver

As for the TPR profiles of Co-Mg-Al-O_x doped with silver, the two main reduction peaks are shifted to lower temperature due to the presence of silver oxide species, which alters significantly the redox properties of Co-Al-O_x.

The amount of silver above 1 wt.% in the samples did not cause further alteration in the reduction temperatures. The material with 0.7 wt.% of silver added during coprecipitation showed the reduction temperature of Co_3O_4 lower by about 20°C, than the respective materiel doped through impregnation. Thus, as for Ag-Co-Mg-Al-O_x, the doping with silver during coprecipitation led to a better dispersion of silver oxide inside Co-Al-O_x.

For the selected materials: CHT-Co_3Al, CHT-Co_3Al + 0.7 wt.% Ag impr., CHT-Co_3Al + 0.7 wt.% Ag copr., CHT-Co_3Al + 1wt.% Ag copr. XPS analyses were carried out, in

order to obtain further information on the surface species of the catalysts' surface. Figure 30 shows the XPS spectra corresponding to the electronic transitions from the Co $2p_{1/2}$ and Co $2p_{3/2}$ orbitals.

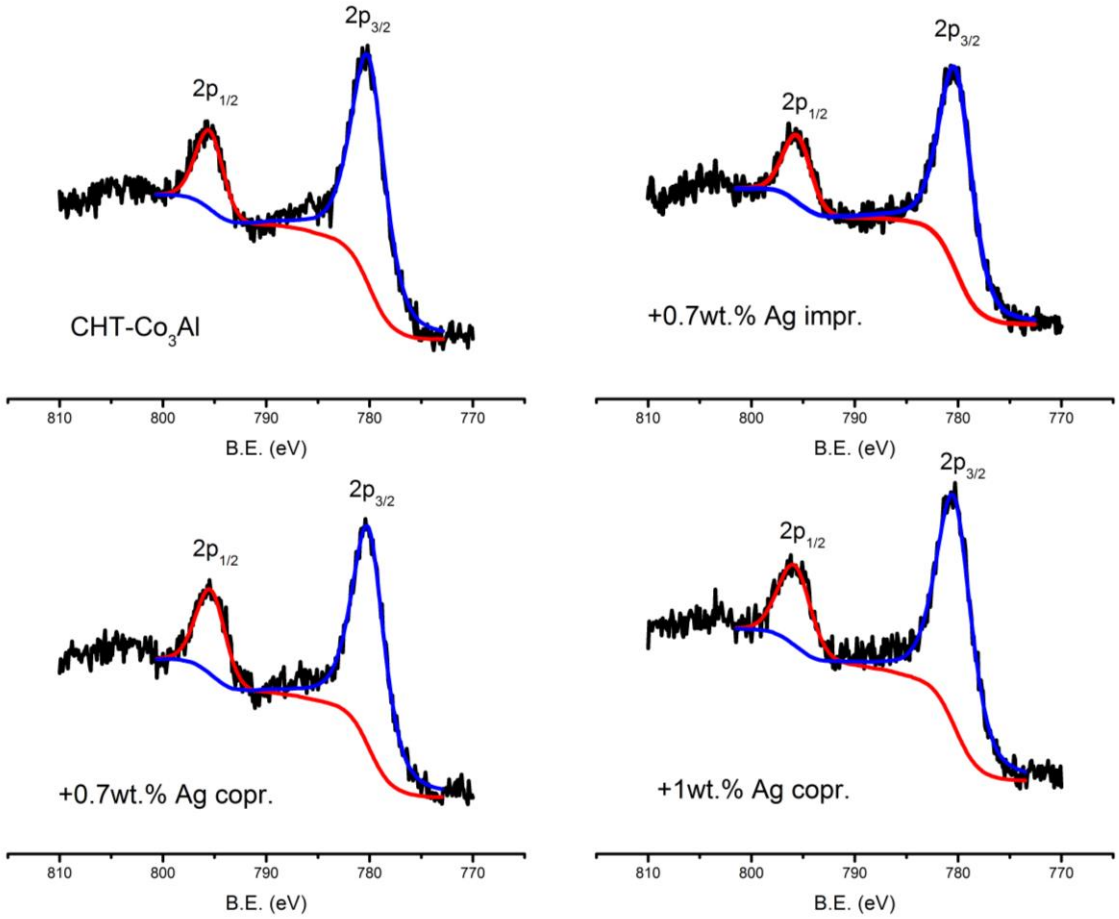

Fig. 30 XPS deconvoluted spectra for Co $2p_{1/2}$ and Co $2p_{3/2}$ orbitals of Co-Al calcined HT-l compounds with various amount of silver

All evaluated samples showed similar spectra, consisting of the two main Co $2p_{3/2}$ and $2p_{1/2}$ peaks, characterized by binding energies in ranges of 780-780.4 and 795.3-795.8 respectively, [82,83] The spin-orbit splitting value for CoO and Co_2O_3 is 16 eV and 15 eV respectively, while for Co_3O_4 is 15.2 ± 1 eV. The samples analysed showed spin-orbit splitting value in the range of 15.35 ± 0.5eV. Thus, only Co_3O_4 and $CoAl_2O_4$, (with spin-orbit splitting value of 15.9 eV.[84]) existed on the catalysts' surface. [85–87] Figure 31 shows the XPS spectra corresponding to the electronic transitions from the Ag $3d_{3/2}$ and Ag $3d_{5/2}$ orbitals.

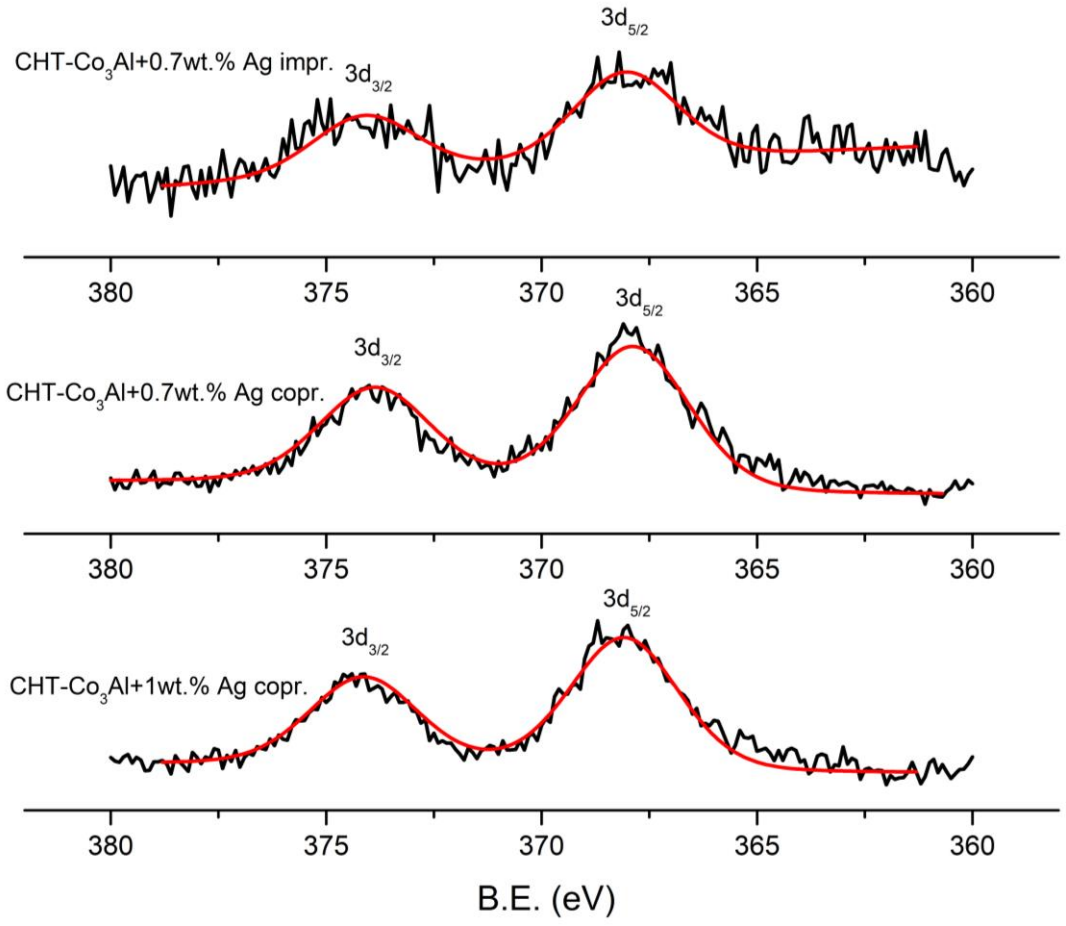

Fig. 31. XPS deconvoluted spectra for Ag $3d_{3/2}$ and Ag $3d_{5/2}$ orbitals of Co-Al calcined HT-l compounds with various amount of silver.

Based on XPS analysis is rather difficult to distinguish the silver oxidation state, since the binding energies of silver in the metallic and in the oxidized form are very close (368.2 eV and 367.9 eV, respectively).[88] However XRD analysis evidenced that a separate Ag_2O phase emerges at higher amount of silver incorporation, thus we can speculate that mainly Ag^+ existed in these samples

Table 3 summarizes the Ag $3d_{5/2}$ binding energies with the respective Ag/Co atomic ratio on the surface of the analyses catalysts.

Table 4 Binding energies (B.E.), peak areas, Full Width at Half Maximum (FWHM) and ratio Ag/Co for Co-Al calcined HT-l with various amounts of silver

Catalysts	B.E. (eV) 3d $_{5/2}$	Area	FWHM	Ag/Co
CHT-Co_3Al +0.7 wt.% Ag impr.	368.1	895	2.88	0.08
CHT-Co_3Al +0.7 wt.% Ag copr.	367.9	3399	3.07	0.27
CHT-Co_3Al +1 wt.% Ag copr.	368.1	4229	2.98	0.31

The Ag/Co atomic ratio of 0.7 wt.%Ag/Co-Al-O_x doped by impregnation was almost 3.5 times lower than the respective one doped by coprecipitation. Thus, most of silver of the impregnated catalyst was diffused into mixed metal oxides structure, possibly during the calcination process.

3.2 Catalytic tests

3.2.1 Calibration of the IR spectrometer

Prior to the reaction tests, the calibration of the IR spectrometer was carried out, in order to check the direct proportion of the peaks area of the IR spectra and the concentration of N_2O in the effluent gas from the reactor. Therefore, a series of IR spectra were recorded, analysing gas flows with different concentrations of N_2O. The flows were regulated by a calibrated mass flow controller, thus with known concentrations of N_2O. The area of the peak at 1298 cm^{-1} related to the N_2O stretching was used for the calibration. Figure 32 presents the result of the calibration.

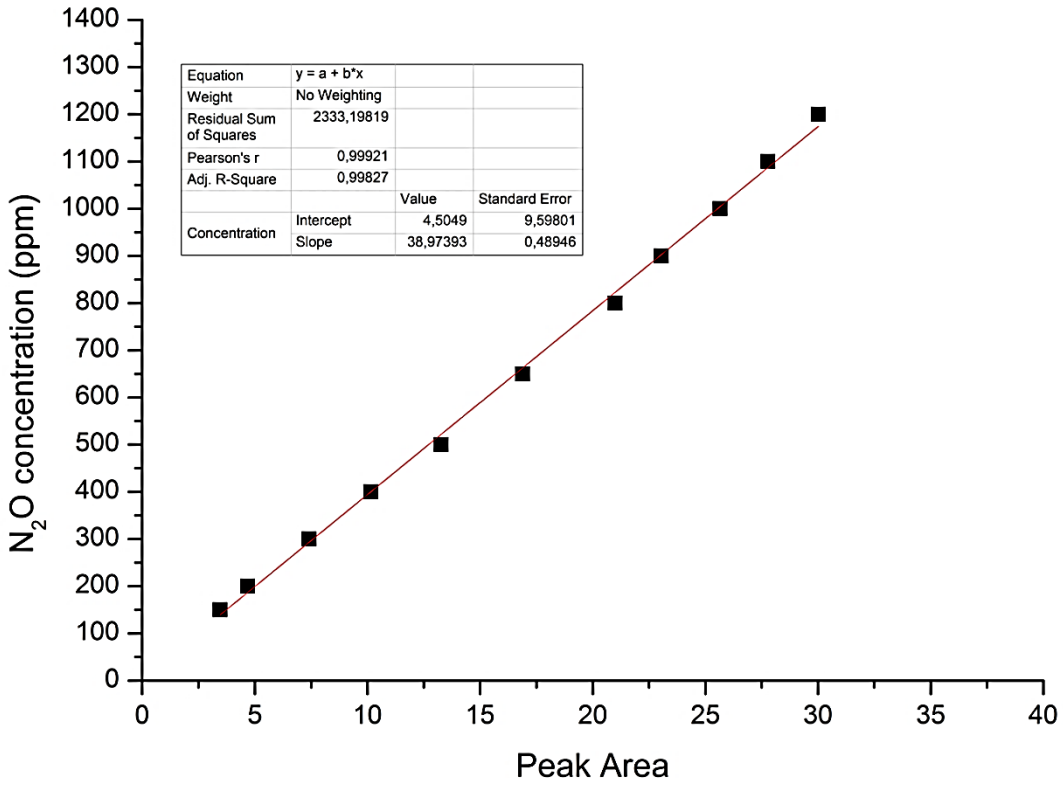

Fig. 32 Plot of N_2O concentration versus the areas of the peaks related to the N_2O stretching

A linear correlation was achieved between the N_2O concentrations and the peaks area. Thus, those areas served for the evaluation of the N_2O conversion.

3.2.2 Test with empty reactor and various weight hours space velocities (WHSV)

The initial tests were carried out with a reactor without the catalytic bed under *ideal conditions*, in the temperature range of 50-600°C (Fig. 33).

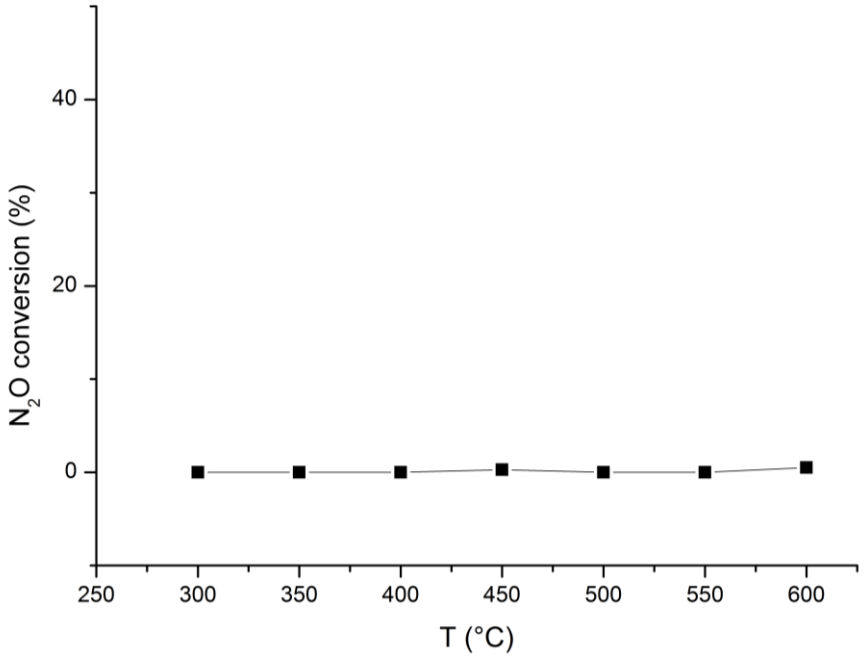

Fig. 33 N_2O conversion in "empty" reactor, reaction conditions: total flow: 100 cm3/min, 0.1 vol.%N_2O, N_2 balance.

Nearly no N_2O conversion was obtained until 600°C in the gas phase.

The first series of catalytic tests were carried out using a catalyst with a fixed molar composition of Co/Al = 3/1 and varying WHSV (Fig. 34).

The activity increased gradually up to a WHSV of 170 L $(h\ g)^{-1}$. Afterwards, the increase of the amount of catalyst to 400 mg (WHSV of 150 L h^{-1} g^{-1}), did not lead to higher activity. Thus, the further catalytic tests were carried out with a WHSV of 170 (350 mg of catalyst and a total flow rate of 100 cm^3/min).

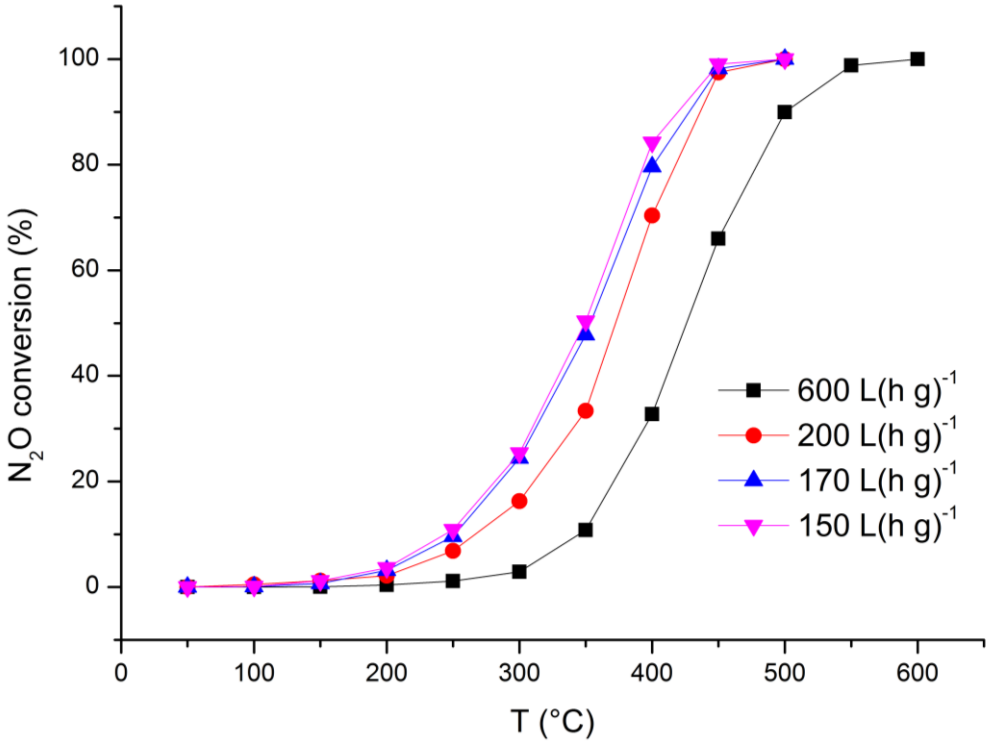

Fig. 34 N_2O conversion with different WHSV, reaction conditions: total flow: 100 cm^3/min, 0.1 vol.%N_2O, N_2 balance.

3.2.3 Catalytic tests over Co(Cu)-(Mg)-Al-O_x

Figure 35 presents the result of the catalytic tests over Co(Cu)-(Mg)-Al-O_x hydrotalcite derived mixed metal oxides.

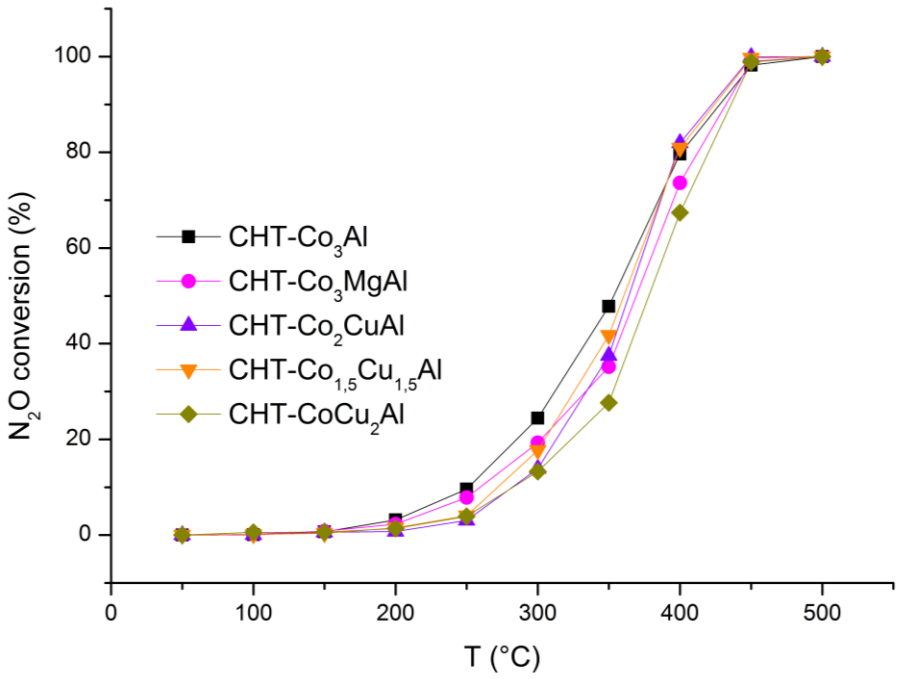

Fig. 35 N_2O conversion of Co-Cu-Mg-Al calcined HT-l compounds, reaction performed under *ideal conditions*

Among all tested materials, CHT-Co_3Al reached the highest activity with a T_{50} (temperature necessary to reach 50% conversion) at 353°C. The activity of Co-Al-O_x decreased after the introduction of copper or magnesium into the structure. However, conversions ≥99% at 450°C were achieved with all the Co(Cu)-(Mg)-Al-O_x catalysts. The lowest activity was showed by the catalyst containing the highest amount of copper (Co/Cu/Al = 1/2/1, mol.%). This effect could be explained by the fact that the increase of the amount of copper in the material caused the decrease of the formation of $Cu_xCo_{1-x}Al_2O_4$, as shown in the TPR profile (Chapter 3.1.2,). Furthermore, Franken *et al.*[25] reported an optimum molar ratio in $Cu_xCo_{3-x}O_4$ of Cu/Co = 1/11, thus the amount of copper in the tested catalysts (Co/Cu/Al = 2/1/1 Co/Cu/Al = 1.5/1.5/1, Co/Cu/Al = 1/2/1 mol.%) was probably too high to notice synergetic effect between cobalt and copper oxides.

On the other side, the lower activity of Co-Mg-Al-Ox (Co/Mg/Al = 3/1/1, mol.%) appeared due to presence of inactive MgO, as reported earlier by J. Perez-Ramirez *et al.*[27,29]

Figure 36 compares the catalytic tests carried out over mixed metal oxides obtained by coprecipitation or thermal decomposition.

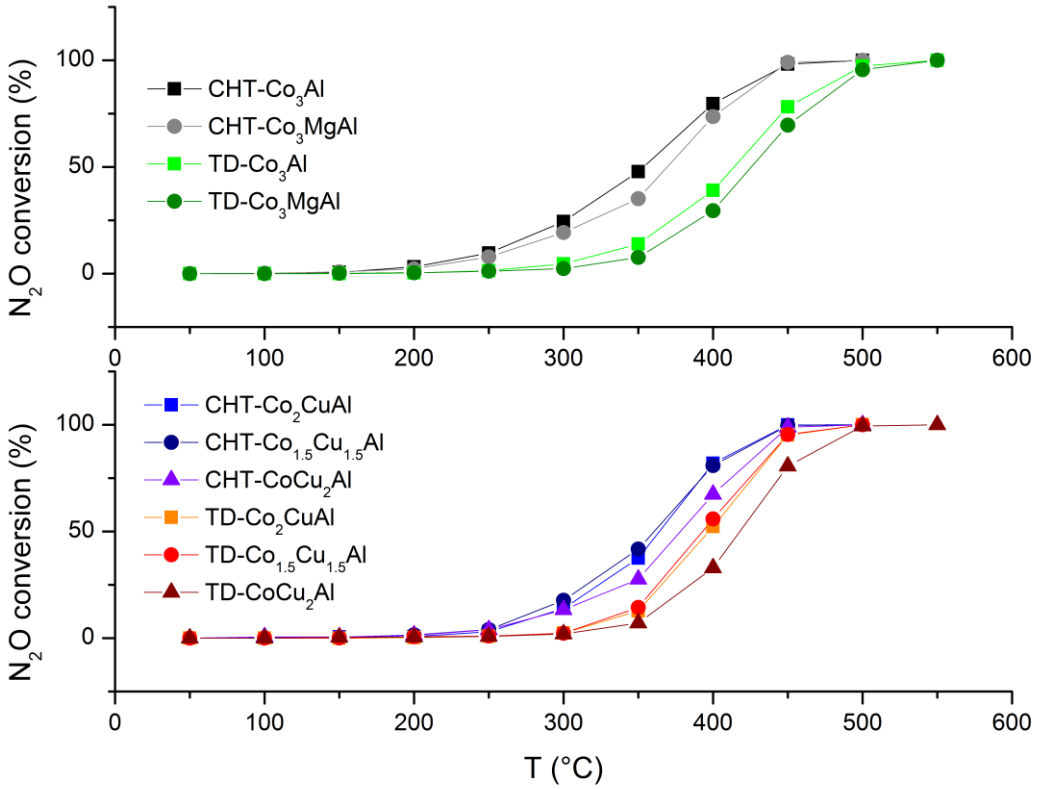

Fig. 36 N_2O conversion of CHT/TD-Co-Cu-Mg-Al, reaction performed under *ideal conditions*

All evaluated hydrotalcite derived mixed metal oxides showed higher activity than analogous materials obtained by thermal decomposition. The low activity for the materials obtained by thermal decomposition appeared possibly due to their significantly lower specific surface areas (as evidenced through N_2 physisorption analysis), compared to the hydrotalcite derived mixed metal oxides. This led to a worse dispersion of cobalt oxide species on the surface of the catalysts, which is a crucial parameter for deN_2O.[9,23]

The differences in activity of deN_2O were significant especially in the intermediate temperatures. E.g. TD-Co_3Al and TD-Co_3MgAl showed a T_{50} around 50°C lower than the respective catalysts obtained from HT-l compounds.

Co(Cu)-(Mg)-Al-O_x hydrotalcite derived mixed metal oxides (Co/Al = 3/1, Co/Mg/Al = 3/1/1, Co/Cu/Al = 2/1/1 Co/Cu/Al = 1.5/1.5/1, Co/Cu/Al = 1/2/1 mol.%) were tested in the presence of O_2 and NO (Fig. 37).

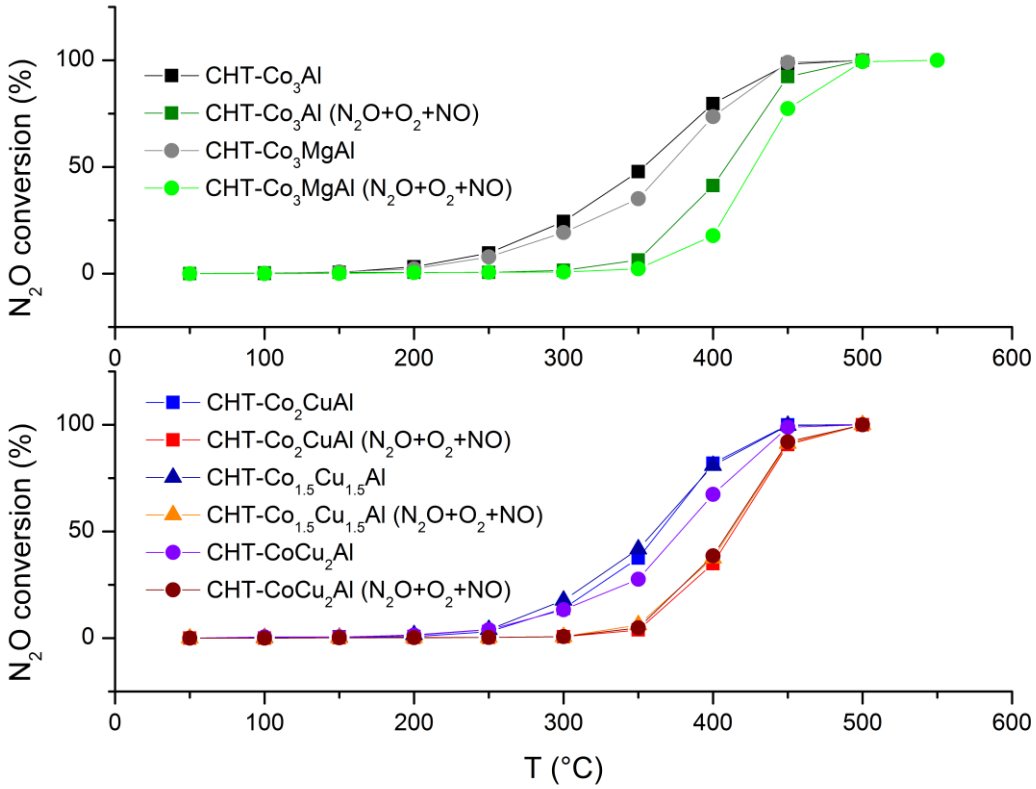

Fig. 37 N_2O conversion on Co-Cu-Mg-Al calcined HT-l compounds, under *ideal condition* or *real conditions* (N_2O+O_2+NO)

The presence of O_2 and NO slightly inhibited the activity of all the catalysts tested, and shifted the conversion curves to higher temperatures of about 50-70°C. The depletion of the activity appeared due to the fact that O_2, as well as NO, can be chemisorbed on the active sites of many catalysts, decreasing their catalytic activity in deN_2O.[9] The N_2O decomposition under *real conditions* started to be significant above 350°C, afterwards the conversion rapidly increased and full conversion is achieved at 500°C. The inhibition in the presence of O_2 and NO in the feed was more significant for CHT-Co_3Al and CHT-Co_3MgAl, which showed a T_{50} lowered of almost 70°C under *real condition*.

3.2.4 Catalytic tests over Ag-doped Co-(Mg)-Al-O_x

In order to evaluate influence of silver-doping, a series of Ag- or Rh-modified Co-(Mg)-Al-O_x (Co/Al = 3/1, Co/Mg/Al = 3/1/1) catalysts were investigated for deN_2O. The first composition was selected because it provided the highest activity during the catalytic tests *under ideal* condition or under *real condition*. The second one, instead, was

selected because MgO, as reported by Perez-Ramirez *et al.*[7,27], improves the stability of the catalysts during time-on-stream tests and in presence of inhibitors such as O_2 and SO_2. Figure 38 compares the catalytic tests carried out over Ag/Rh-Co-(Mg)-Al-O_x modified during coprecipitation or trough impregnation.

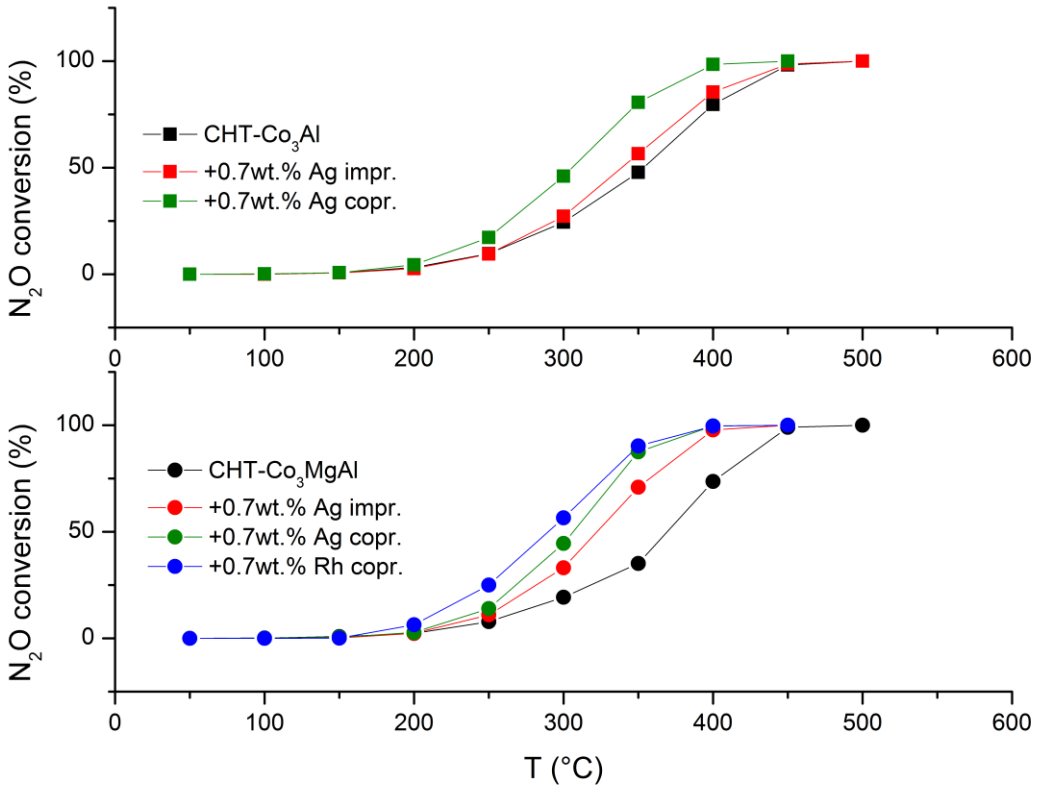

Fig. 38 N_2O conversion over Ag- or Rh modified Co-Mg-Al calcined HT-l compounds doped during coprecipitation (copr.) or through impregnation (impr.), reaction performed under *ideal conditions*

The modification with silver influenced significantly the activity of Co-(Mg)-Al-O_x, and led to nearly full N_2O conversions at 400°C. As evidenced from TPR results, the presence of Ag in Co-mixed oxides increased the reducibility of cobalt, which plays an important role in de N_2O.[89] Apparently, the modification with silver weakened the Co-O bond, in a way similar to the alkali metal-doping, and promoted the oxygen desorption from the surface of the catalysts.[90,91]

Ag-Co-Al-(Mg)-O_x doped during coprecipitation showed the highest activity, probably due to a uniform dispersion of silver oxide species in these materials. The XPS results revealed relatively low amount/ratio of the silver oxide species for impregnated materials. Thus possibly, most of them were diffused inside the structure after calcination step. Additionally, as evidenced by H_2-TPR analysis, the Ag-Co-(Mg)-Al-Ox doped during coprecipitation showed enhanced reducibility compared to the

impregnated materials. As evidenced by H_2-TPR analysis, the Rh-doped catalysts showed the lowest reduction temperature and thus, the highest activity.

In the next step, the effect of different loading of silver on activity in deN_2O was evaluated for Co-Al-O_x and Co-Mg-Al-O_x hydrotalcite derived mixed metal oxides (Fig. 39).

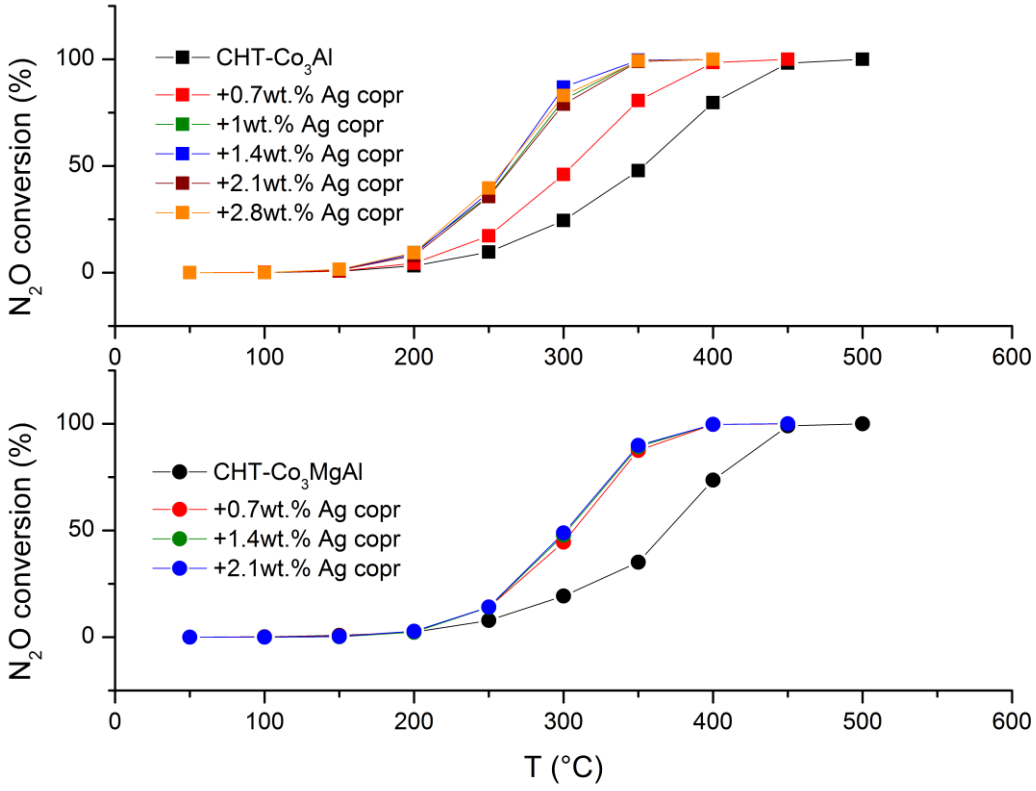

Fig. 39 N_2O conversion over Co-Mg-Al calcined HT-l compounds modified with different amounts of silver, reaction performed under *ideal conditions*

In case of catalysts containing Mg - Co-Mg-Al-O_x - the increase of Ag loading caused no significant changes in the activity. On the other hand, a gradual increase of activity was noticed for Co-Al-O_x with increasing silver loading up to 1 wt.%. A higher amount of silver (≥ 1 wt.%) did not result in higher activity. The results were in agreement with TPR results, that evidenced no further alteration of cobalt reducibility for materials with silver above 1 wt.%. Therefore the optimum composition was found for (1 wt.% Ag)CHT-Co_3Al, which revealed nearly full conversion at 350°C.

Figure 40 shows the catalytic tests over silver-modified materials in presence of O_2 and NO in the feed.

Again, the presence of O_2 and NO slightly inhibited the activity. However, a conversion of 88% was obtained over (1 wt.% Ag)CHT-Co_3Al at 400°C. Besides, the activity of

Rh-doped catalyst was negatively affected by the presence of O_2 and NO in the feed gas. Consequently, under *real conditions*, no significant difference in activity appeared between materials modified with both Ag or Rh

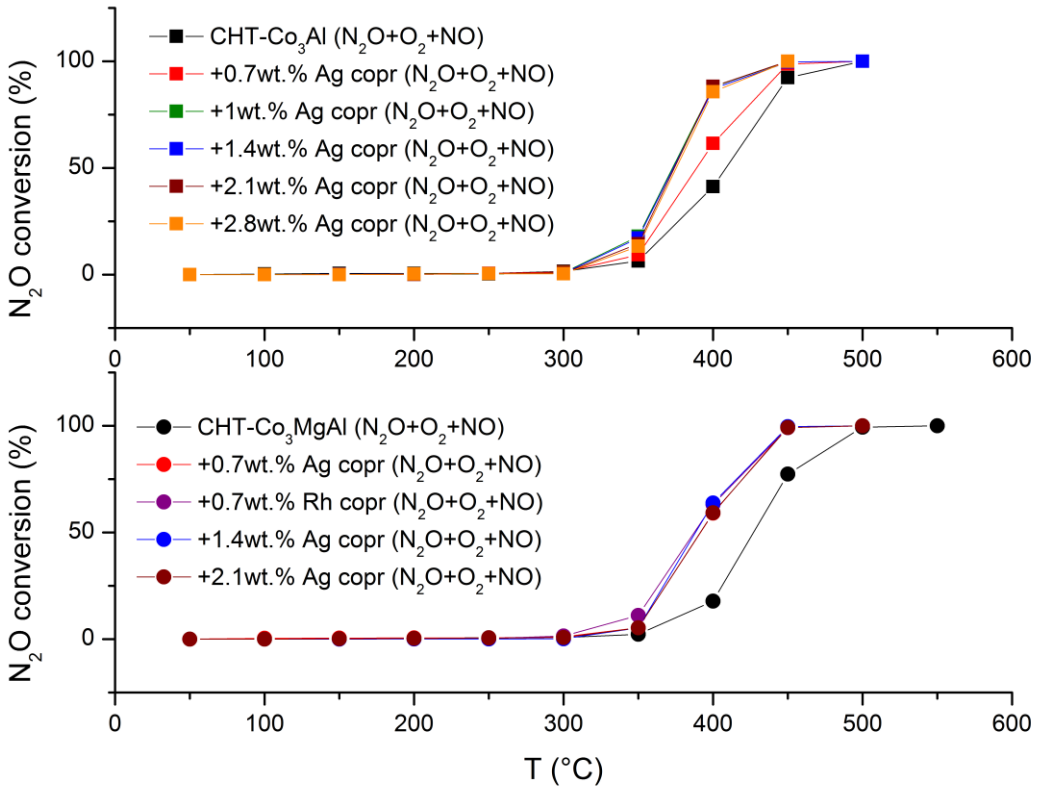

Fig. 40 N_2O conversion over Co-Mg-Al calcined HT-l compounds modified with different amounts of silver, reaction performed under *ideal conditions* or under *real conditions* (N_2O+O_2+NO)

3.2.5 Catalytic tests over (1 wt.% Ag)CHT-Co_3Al

Figure 41 presents the results of catalytic tests in the presence of O_2 and additionally NO over (1 wt.% Ag)CHT-Co_3Al.

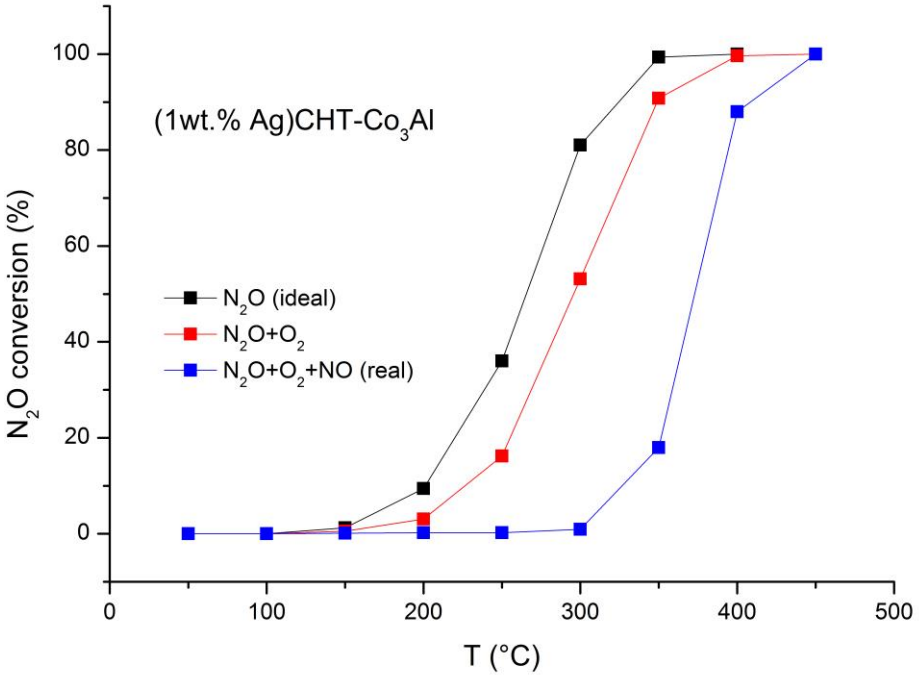

Fig. 41 N_2O conversion over (1 wt.% Ag)CHT-Co_3Al, reaction performed under *ideal conditions, real conditions* (N_2O+O_2+NO) or in presence of O_2

The tested catalyst suffered from O_2 inhibition: the presence of O_2 slightly decreased the activity of (1 wt.% Ag)CHT-Co_3Al, lowering the T_{50} of almost 50°C. Thus, O_2 was probably adsorbed on the active sites (*) of the catalysts, through a dissociative adsorption process (Eq. 19,20):[8,9,15]

$$O_2 + * \rightarrow O_2* \quad (19)$$

$$O_2* + * \rightarrow 2O* \quad (20)$$

The co-existence of O_2 and NO dramatically reduced the catalytic activity below 400°C, probably due to a synergetic effect of competition with N_2O for the active sites of the catalyst. Under *real condition*, in fact, the N_2O conversion started to be significant only above 300°C, while full conversion was achieved at 450°C.

Figure 42 presents the stability test over (1 wt.% Ag)CHT-Co_3Al, carried out for 30 h under *real conditions* at 400°C. The catalyst showed a maximum of conversion (92%) during the first 5 hours, afterwards, a stable conversion of 87-89% appeared. Thus (1 wt.% Ag)CHT-Co_3Al showed high stability within 30 h of exposure to a mixture of N_2O, O_2 and NO without deactivation.

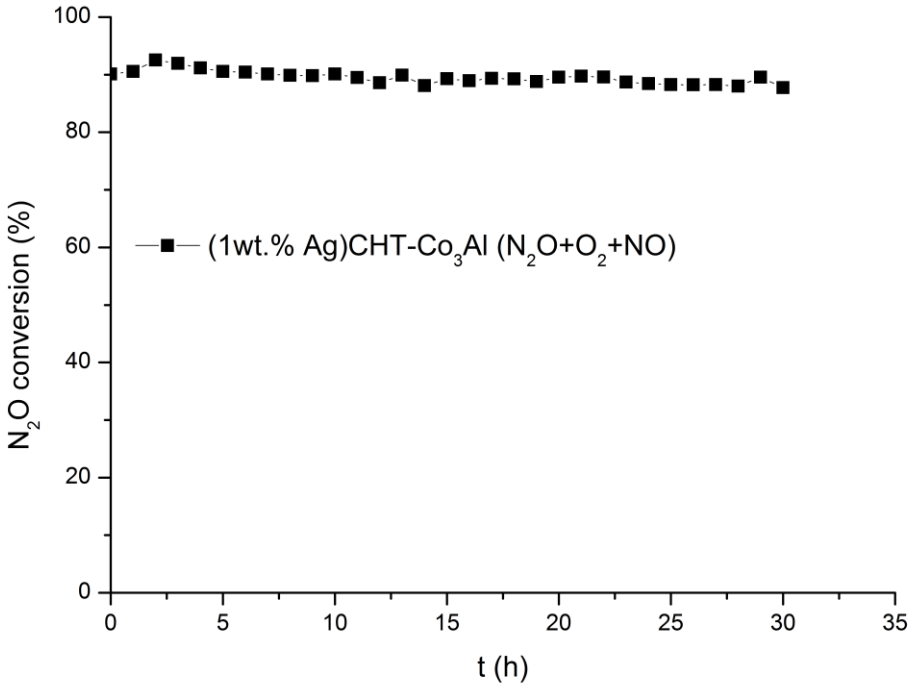

Fig. 42 N_2O conversion over (1 wt.% Ag)CHT-Co_3Al, reaction performed under *real conditions* (N_2O+O_2+NO) T: 400°C

3.2.6 Catalytic tests with H_2-pretreatment

The last series of catalytic tests were devoted to the evaluation of activity for *in situ* H_2-pretreated (5.0 vol.% H_2 diluted in Ar) materials. Figure 43 shows the results of the catalytic tests carried out after H_2-pretreatment over (0.7 wt.% Ag impr.)CHT-Co_3Al, (0.7 wt.% Ag copr.)CHT-Co_3Al, (1 wt.% Ag copr.)CHT-Co_3Al and (2.8 wt.%Ag impr.)/Al_2O_3.

(2.8 wt.% Ag impr.)/Al_2O_3 showed improved activity after the *in situ* pretreatment. In particular, the T_{50} is lowered from 500 °C to 450°C after the H_2-pretreatment. However, the conversion is still lower than Co-based catalysts.

Also Ag-Co-Al-O_x showed enhanced activity after the H_2-pretreatment, providing significant conversions already below 100°C. (1 wt.% Ag copr.)CHT-Co_3Al showed the highest activity with a conversion of 69% at 100°C and full conversion at 250°C. These results could have two possible explanations:

(i) *in situ* H_2-pretreatment led to the formation of reduced species, such as $Ag_n^{\delta+}$ clusters, highly active for deN_2O, and/or

(ii) molecules of H_2 adsorbed during pretreatment, and enhanced the removal of $O_{(ads)}$ molecules on the catalysts' surface during deN_2O.

However, silver oxide is not the only species that can be reduced during H_2-pretreatment, as evidenced from TPR profiles in the chapter 3.1.2. Thus, this section needs further investigation, such as a comprehensive study on the effect of the H_2-pretreatment on the physicochemical properties of Ag-modified Co-Al-O_x.

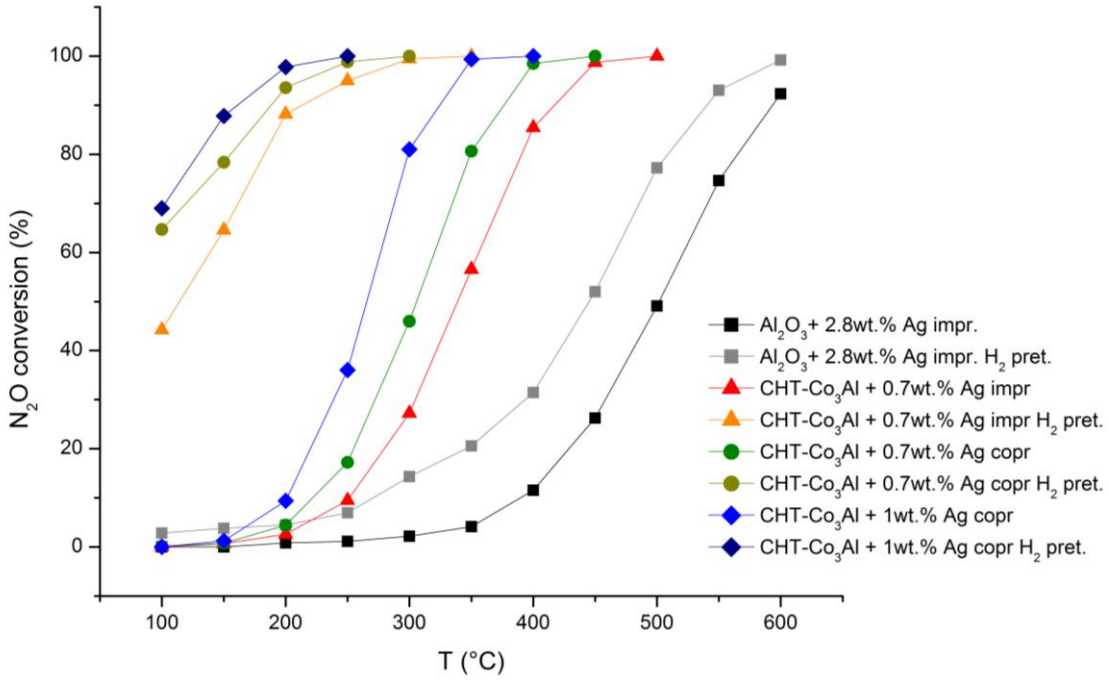

Fig. 43 N_2O conversion of HT-Co_3Al modified with different amounts of silver and Al_2O_3 + 2.8wt.%Ag impr., with and without H_2 pretreatment, reaction performed under *ideal conditions*

3.2.7 Summary

A great variety of catalysts were tested for N_2O decomposition under *ideal conditions* (N_2O,N_2) and *real conditions* (N_2O/O_2/NO,N_2), respectively. Figure 44 summarizes the light-off temperatures (T_{50}) for Co(Cu)-(Mg)-Al-Ox obtained by coprecipitation or thermal decomposition.

Among all evaluated materials, Co-Al-O_x with molar ratio Co/Al = 3/1 hydrotalcite derived mixed metal oxides showed a T_{50} of 353 °C and 409 °C under both *ideal condition* and *real condition*, respectively. On the other hand, introducing of copper and magnesium resulted in significant lower activity in deN_2O. The materials obtained by thermal decomposition shower poor activity with T_{50} > 390 °C under *ideal conditions*.

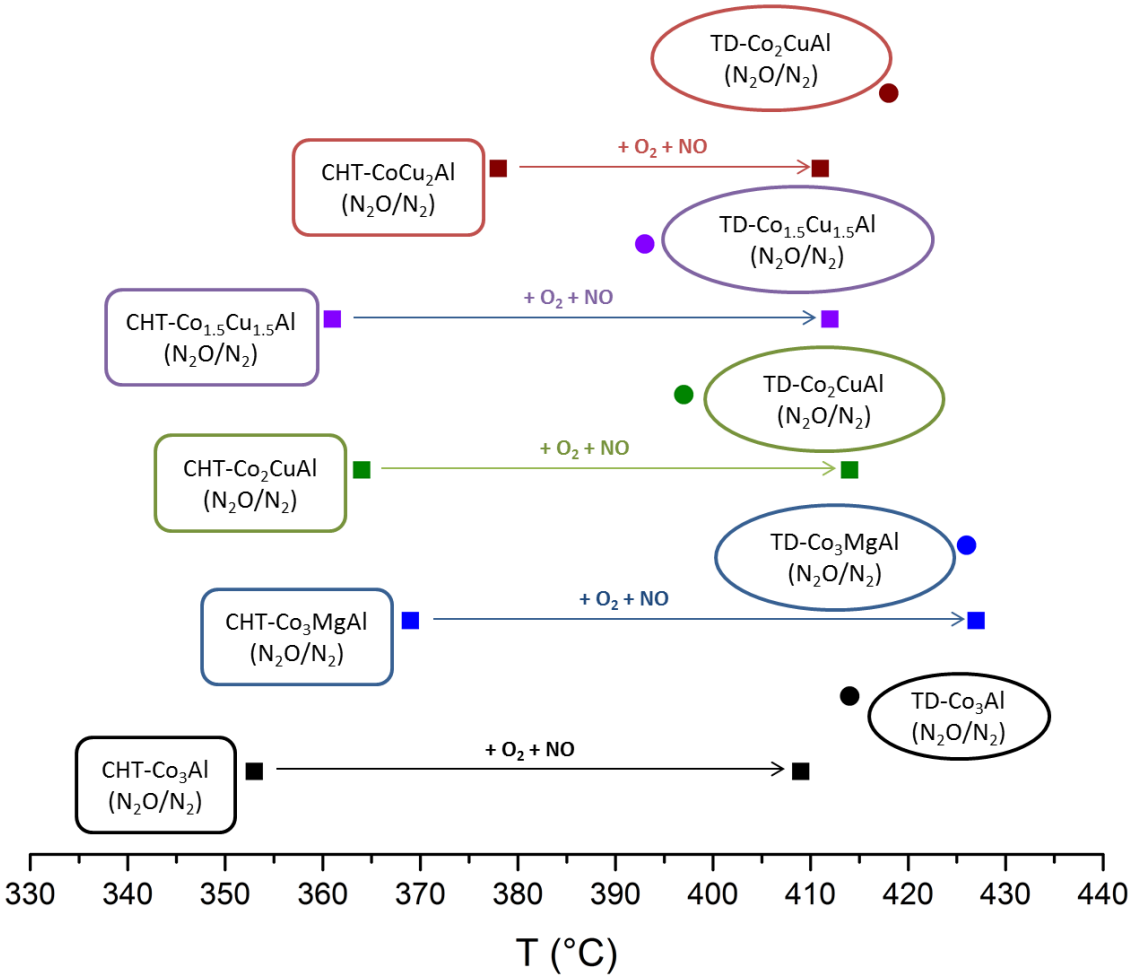

Fig. 44 Summary of T_{50} for undoped Co(Cu)-Mg-Al catalysts under *ideal condition* or *real condition*

Figure 45 summarizes the T_{50} obtained from the catalytic tests for Ag- or Rh-doped Co-Al-Ox and Co-Mg-Al-O_x (Co/Al = 3/1, Co/Mg/Al = 3/1/1). Among the Ag-modified materials, (1 wt.% Ag)CHT-Co_3Al reached the highest activity with a T_{50} of 266 °C and 373 °C under *ideal conditions* and *real conditions*, respectively.

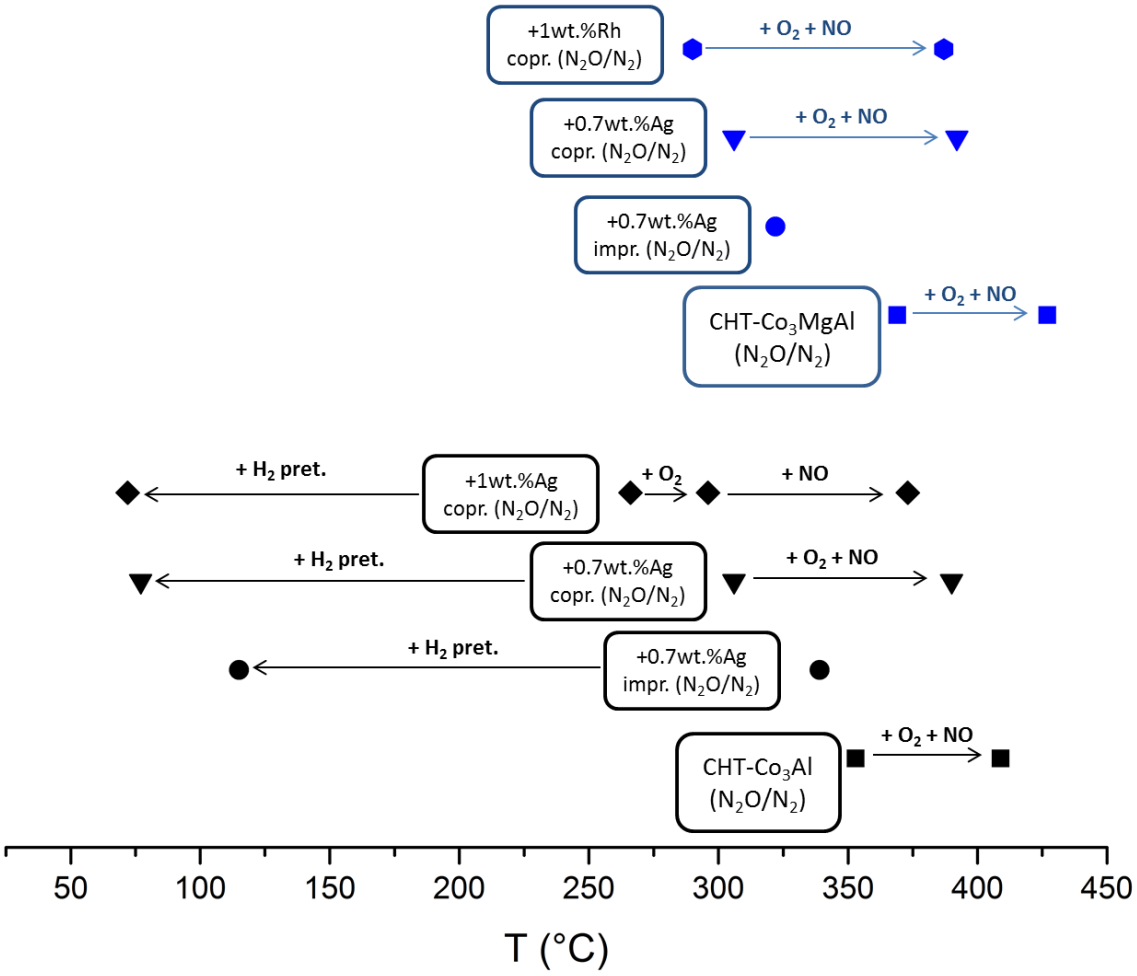

Fig. 45 Summary of T_{50} for Ag- or Rh-modified Co(Cu)-Mg-Al calcined HT-l compounds under *ideal condition* or *real condition*

Chapter 4: Conclusions

Co-Al-O_x mixed metal oxides partially modified with Cu or Mg, as well as Ag were successfully prepared, characterized and evaluated as potential catalysts for the N_2O decomposition.

Firstly, Co(Cu)-(Mg)-Al HT-l compounds with intended molar ratios were prepared by coprecipitation. Co(Cu)-(Mg)-Al-O_x were obtained from (i) calcination of HT-l compounds or (ii) thermal decomposition of aqueous solution containing the nitrates of the desired metals. The catalytic tests underlined the superior activity of HT derived mixed metal oxides, probably due to their higher specific surface area. Among the HT-originated catalysts, the activity decreased in the order: Co_3Al > $Co_{1.5}Cu_{1.5}Al$ > Co_2CuAl > Co_3MgAl > $CoCu_2Al$. Catalytic test under *real conditions* (in presence of O_2 and NO) evidenced slight inhibition of the activity for all the catalysts.

Afterwards, the compositions Co/Al = 3/1 and Co/Mg/Al = 3/1/1, mol.% were chosen to prepare Ag-modified HT-derived mixed oxides. Silver influenced the redox properties of the doped materials, increasing the reducibility of cobalt, as evidenced from H_2-TPR analysis. Ag-Co-(Mg)-O_x showed enhanced activity compared to the undoped materials, in particular (1 wt.% Ag)HT-Co_3Al was the most promising (T_{50} of 266 °C under *ideal conditions*). The activity varied also depending on the modification methods: Ag-doping during coprecipitation led to a uniform dispersion of silver species on the surface of the material, providing the best catalytic performances. However, the presence of O_2 and NO still inhibited the activity of Ag-modified HT-derived mixed oxides, due to a synergetic effect of competition with N_2O for the active sites of the catalyst (T_{50} of 373 °C under *real conditions* for 1 wt.% Ag/CHT-Co_3Al). For the most active catalysts (1 wt.% Ag/CHT-Co_3Al) an additional stability test was carried out. The test evidenced high stability and no deactivation of the catalyst within 30 h of exposure to a mixture of N_2O, NO and O_2.

Finally, for a selected group of Ag-modified HT-derived mixed oxides, a series of catalytic tests were carried out applying with *in situ* H_2-pretreatment. The pretreatment significantly improved the activity of the catalysts, even at T < 100°C. This enhancement was probably due to the formation of highly active reduced species during the pretreatment, e.g. $Ag_n^{\delta+}$ clusters. However, this assumption needs further investigations, since silver was not the only species that could be reduced during the H_2-pretreatment.

Although lots of efforts were already done in order to develop satisfactory deN_2O catalyst, N_2O abatement still remains one of the biggest environmental challenge of the twenty-first century. The results obtained in this thesis are undoubtedly interesting, since it was evidenced the possibility to develop a very promising class of materials for deN_2O. The modification of HT-derived mixed oxides with small amounts of silver led to suitably active and stable catalysts with potential technical applications. This could be certainly a starting point for further studies, which may be focused on the research of new type of materials and additional investigations on the role of silver and other promoters inside mixed oxides.

Chapter 5: Bibliography

1. Zuck, D., Ellis, P. & Dronsfield, A. Nitrous oxide : are you having a laugh ? *Educ. Chem.* 26–29 (2012).
2. K. Swezey. Popular Science, 1949, 154, 236-238.
3. Gaidei, T. P. Nitrous oxide: Properties, producing, grounds of manipulations, and fields of application. *Russ. J. Appl. Chem.* **82,** 1689–1705 (2009).
4. UNEP. *Drawing Down N2O To Protect Climate and the Ozone Layer*. (2013). doi:978-92-807-3358-7
5. Konsolakis, M. Recent Advances on Nitrous Oxide (N2O) Decomposition over Non-Noble-Metal Oxide Catalysts: Catalytic Performance, Mechanistic Considerations, and Surface Chemistry Aspects. *ACS Catal.* **5,** 6397–6421 (2015).
6. Breidenich, C. *et al.* The Kyoto Protocol to the United Nations Framework Convention on Climate Change Published by : American Society of International Law. **92,** 315–331 (2015).
7. Perez-Ramirez, J., Kapteijn, F., Mul, G., Xu, X. & Moulijn, J. A. Ex-framework FeZSM-5 for control of N2O in tail-gases. *Catalysis Today* **76,** 55–74 (2002).
8. Pérez-Ramírez, J., Kapteijn, F., Schöffel, K. & Moulijn, J. A. Formation and control of N2O in nitric acid production: Where do we stand today? *Appl. Catal. B Environ.* **44,** 117–151 (2003).
9. Kapteijn, F., Rodriguez-Mirasol, J. & Moulijn, J. A. Heterogeneous catalytic decomposition of nitrous oxide. *Appl. Catal. B Environ.* **9,** 25–64 (1996).
10. Karlsen, E. J., Nygren, M. a. & Pettersson, L. G. M. Theoretical Study on the Decomposition of N2O over Alkaline Earth Metal-Oxides: MgO−BaO. *The Journal of Physical Chemistry A* **106,** 7868–7875 (2002).
11. Sciences, A., Taniou, P. & Ziaka, Z. Catalytic Decomposion of N2O : Best Achievable Methods and Processes. **2,** 149–188 (2013).
12. Ivanov, D. V., Sadovskaya, E. M., Pinaeva, L. G. & Isupova, L. A. Influence of oxygen mobility on catalytic activity of La-Sr-Mn-O composites in the reaction of high temperature N2O decomposition. *J. Catal.* **267,** 5–13 (2009).
13. Li, Y. & Armor, J. N. Catalytic decomposition of nitrous oxide on metal exchanged zeolites. *Appl. Catal. B, Environ.* **1,** 1–9 (1992).
14. Kondratenko, E. V., Kraehnert, R., Radnik, J., Baerns, M. & Pérez-Ramírez, J.

Distinct activity and time-on-stream behavior of pure Pt and Rh metals and Pt-Rh alloys in the high-temperature N2O decomposition. *Appl. Catal. A Gen.* **298,** 73–79 (2006).

15. Centi, G. *et al.* Novel catalysts and catalytic technologies for N2O removal from industrial emissions containing O2, H2O and SO2. *Adv. Environ. Res.* **4,** 325–338 (2000).
16. Tzitzios, V. K. & Georgakilas, V. Catalytic reduction of N2O over Ag-Pd/Al2O3 bimetallic catalysts. *Ag–Pd/Al2O3 Chemosph. bimetallic* **59,** 887–91 (2005).
17. Kumar, A. S. R. I. H., Venkateshwarlu, V., Rao, K. S. R., Lingaiah, N. & Prasad, P. S. S. A. I. Alumina Supported Silver Lanthana Catalyst for N2O Decomposition. **2,** 114–122 (2013).
18. T. N. Angelidis† and V. Tzitzios* Department. Promotion of the Catalytic Activity of a Ag/Al2O3 Catalyst for N2O Decomposition by the Addition of Rh. A Comparative Activity and Kinetic Study. *Dep. Chem. Box 116, Aristotle Univ. Thessaloniki GR-54124, Greece* **42,** 253–259 (2003).
19. Cavani, F., Trifiro, F. & Vaccari, A. Hydrotalcite type anionic clays: Preparation, properties and applications. *Catal. Today* **11,** 173–301 (1991).
20. Vaccari, A. Clays and catalysis: A promising future. *Appl. Clay Sci.* **14,** 161–198 (1999).
21. Jabłońska, M. & Palkovits, R. Nitrogen oxide removal over hydrotalcite-derived mixed metal oxides. *Catal. Sci. Technol.* **6,** 49–72 (2016).
22. Kannan, S. Decomposition of nitrous oxide over the catalysts derived from hydrotalcite-like compounds. *Appl. Clay Sci.* **13,** 347–362 (1998).
23. Kannan, S. & Swamy, C. S. Catalytic Decomposition of Nitrous Oxide over Calcined Cobalt Aluminum Hydrotalcites. *Catal. Today* **53,** 725–737 (1999).
24. Chmielarz, L. *et al.* An influence of thermal treatment conditions of hydrotalcite-like materials on their catalytic activity in the process of N2O decomposition. *J. Therm. Anal. Calorim.* **105,** 161–170 (2011).
25. Franken, T. & Palkovits, R. Investigation of potassium doped mixed spinels CuxCo3-xO4 as catalysts for an efficient N2O decomposition in real reaction conditions. *Applied Catalysis B: Environmental* **176–177,** 298–305 (2015).
26. Chmielarz, L. *et al.* Total oxidation of selected mono-carbon VOCs over hydrotalcite originated metal oxide catalysts. *Catal. Commun.* **17,** 118–125 (2012).

27. Pérez-Ramírez, J., Overeijnder, J., Kapteijn, F. & Moulijn, J. A. Structural promotion and stabilizing effect of Mg in the catalytic decomposition of nitrous oxide over calcined hydrotalcite-like compounds. *Appl. Catal. B Environ.* **23,** 59–72 (1999).
28. Perez-Ramirez, Kapteijn & Moulijn. High activity and stability of the Rh-free Co-based ex-hydrotalcite containing Pd in the catalytic decomposition of N2O. *Catal. Letters* **60,** 133–138 (1999).
29. Pérez-Ramírez, J., Mul, G., Xu, X., Kapteijn, F. & Moulijn, J. A. Co-based ex-HTlc for the decomposition of N2O : Tailoring catalysts for active and stable operation. *Studies in Surface Science and Catalysis* **130,** 1445–1450 (2000).
30. Obalová, L. *et al.* Catalytic decomposition of nitrous oxide over catalysts prepared from Co/Mg-Mn/Al hydrotalcite-like compounds. *Appl. Catal. B Environ.* **60,** 289–297 (2005).
31. Kovanda, F. *et al.* Mixed oxides obtained from Co and Mn containing layered double hydroxides: Preparation, characterization, and catalytic properties. *Journal of Solid State Chemistry* **179,** 812–823 (2006).
32. Obalovà, L. *et al.* Effect of Mn/Al ratio in Co-Mn-Al mixed oxide catalysts prepared from hydrotalcite-like precursors on catalytic decomposition of N2O. *Catalysis Today* **119,** 233–238 (2007).
33. Obalovà, L., Karàskovà, K., Jiràtovà, K. & Kovanda, F. Effect of potassium in calcined Co-Mn-Al layered double hydroxide on the catalytic decomposition of N2O. *Appl. Catal. B Environ.* **90,** 132–140 (2009).
34. Karàskovà, K., Obalovà, L., Jiràtovà, K. & Kovanda, F. Effect of promoters in Co-Mn-Al mixed oxide catalyst on N2O decomposition. *Chem. Eng. J.* **160,** 480–487 (2010).
35. Armor, J. N. *et al.* Calcined hydrotalcites for the catalytic decomposition of N2O in simulated process streams. *Appl. Catal. B Environ.* **7,** 397–406 (1996).
36. Xue, L., Zhang, C., He, H. & Teraoka, Y. Catalytic decomposition of N2O over CeO2 promoted Co3O4 spinel catalyst. *Appl. Catal. B Environ.* **75,** 167–174 (2007).
37. Pacultová, K. *et al.* K-Doped Co–Mn–Al Mixed Oxide Catalyst for N2O Abatement from Nitric Acid Plant Waste Gases: Pilot Plant Studies. *Ind. Eng. Chem. Res.* **55,** 7076–7084 (2016).
38. Angelidis, T. N. & Kruse, N. Promotional effect of SO2 on the selective catalytic

reduction of NOx with propane/propene over Ag/Al2O3. *Applied Catalysis B: Environmental* **34,** 201–212 (2001).

39. Masuda, K., Tsujimura, K., Shinoda, K. & Kato, T. Silver-promoted catalyst for removal of nitrogen oxides from emission of diesel engines. *Appl. Catal. B Environ.* **8,** 33–40 (1996).
40. Masuda, K., Shinoda, K., Kato, T. & Tsujimura, K. Activity enhancement of Ag/mordenite catalysts by addition of palladium for the removal of nitrogen oxides from diesel engine exhaust gas. *Appl. Catal. B Environ.* **15,** 29–35 (1998).
41. Miyadera, T. Alumina-Supported Silver Catalysts for the Selective Reduction of Nitric-Oxide With Propene and Oxygen-Containing Organic-Compounds. *Appl. Catal. B-Environmental* **2,** 199–205 (1993).
42. Angelidis, T. N., Christoforou, S., Bongiovanni, A. & Kruse, N. On the promotion by SO2 of the SCR process over Ag/Al2O3: Influence of SO2 concentration with C3H6 versus C3H8 as reductant. *Appl. Catal. B Environ.* **39,** 197–204 (2002).
43. Matsuoka, M., Ju, W. S., Yamashita, H. & Anpo, M. In situ characterization of the Ag+ ion-exchanged zeolites and their photocatalytic activity for the decomposition of N2O into N2 and O2 at 298 K. *Journal of Photochemistry and Photobiology A: Chemistry* **160,** 43–46 (2003).
44. Kočí, K., Krejčíková, S., Šolcová, O. & Obalová, L. Photocatalytic decomposition of N2O on Ag-TiO2. *Catal. Today* **191,** 134–137 (2012).
45. Ramnani, S. P. *et al.* Advantage of radiolysis over impregnation method for the synthesis of SiO2 supported nano-Ag catalyst for direct decomposition of N2O. *Catal. Commun.* **9,** 756–761 (2008).
46. Sano, T., Negishi, N., Mas, D. & Takeuchi, K. Photocatalytic Decomposition of N2O on Highly Dispersed Ag+ Ions on TiO2 Prepared by Photodeposition. *J. Catal.* **194,** 71–79 (2000).
47. Tzitzios, V. K., Georgakilas, V. & Angelidis, T. N. Catalytic reduction of N 2 O with CH 4 and C 3 H 6 over Ag – Rh / Al 2 O 3 bimetallic catalyst in the presence of oxygen. **704,** 699–704 (2005).
48. Konkol, M. *et al.* Decomposition of the mixed-metal coordination polymer — A preparation route of the active Ag/Yb2O3 catalyst for the deN2O process. *'Applied Catalysis B, Environmental'* **190,** 85–92 (2016).
49. Liu, Z., Hao, J., Fu, L. & Zhu, T. Study of Ag/La0.6Ce0.4CoO3 catalysts for

direct decomposition and reduction of nitrogen oxides with propene in the presence of oxygen. *Applied Catalysis B: Environmental* **44,** 355–370 (2003).

50. Kumar, S., Teraoka, Y., Joshi, A. G., Rayalu, S. & Labhsetwar, N. Journal of Molecular Catalysis A : Chemical Ag promoted La0.8Ba0.2MnO3 type perovskite catalyst for N2O decomposition in the presence of O2 , NO and H2O. *'Journal of Molecular Catalysis. A, Chemical'* **348,** 42–54 (2011).
51. Zhao, S. & Li, J. Silver-Cobalt Oxides Derived from Silver Nanoparticles Deposited on Layered Double Hydroxides for Methane Combustion. *ChemCatChem* **7,** 1966–1974 (2015).
52. Shibata, J. *et al.* Structure of active Ag clusters in Ag zeolites for SCR of NO by propane in the presence of hydrogen. *J. Catal.* **227,** 367–374 (2004).
53. Shimizu, K., Tsuzuki, M., Kato, K., Yokota, S. & Okumura, K. Reductive Activation of O2 with H2 -Reduced Silver Clusters as a Key Step in the H2 -Promoted Selective Catalytic Reduction of NO with C3H8 over Ag/ Al2O3. *J. Phys. Chem. C* **111,** 950–959 (2007).
54. Satokawa, S., Shibata, J., Shimizu, K. I., Satsuma, A. & Hattori, T. Promotion effect of H2 on the low temperature activity of the selective reduction of NO by light hydrocarbons over Ag/Al2O3. *Appl. Catal. B Environ.* **42,** 179–186 (2003).
55. Satokawa, S. *et al.* Promotion effect of hydrogen on lean reduction by hydrocarbons over catalyst. *Chem. Eng. Sci.* **62,** 5335–5337 (2007).
56. WICHTERLOVA, B. *et al.* An in situ UV–vis and FTIR spectroscopy study of the effect of H and CO during the selective catalytic reduction of nitrogen oxides over a silver alumina catalyst. *J. Catal.* **235,** 195–200 (2005).
57. Burch, R., Daniells, S. T., Breen, J. P. & Hu, P. The Effect of H2 and the Presence of hot-O(ads) During the Decomposition of N2O on Platinum. *Catalysis Letters* **92,** 103–108 (2004).
58. Carabineiro, S. A. & Nieuwenhuysd, B. E. Reduction of N2O by H2 on the Ir(1 1 0) surface: oscillations in rate. *Energy & Fuels* **495,** 1–7 (2001).
59. Kondratenko, E. V., Kondratenko, V. A., Richter, M. & Fricke, R. Influence of O2 and H2 on NO reduction by NH3 over Ag/Al2O3: A transient isotopic approach. *Journal of Catalysis* **239,** 23–33 (2006).
60. Kondratenko, V. A., Bentrup, U., Richter, M., Hansen, T. W. & Kondratenko, E. V. Mechanistic aspects of N2O and N2 formation in NO reduction by NH3 over Ag/Al2O3: The effect of O2 and H2. *Appl. Catal. B Environ.* **84,** 497–504

(2008).

61. Barbara L Dutrow, Louisiana State University , Christine M. Clark, E. M. U. X-ray Powder Diffraction (XRD). *Geochemical Instrumentation and Analysis*
62. diffrazione-dei-raggi-x @ www.chimicamo.org.
63. Splettstoesser, T. *Structure determination by X-ray crystallography*. (2006).
64. Coats, A. W. & Redfern, J. P. Thermogravimetric Analysis. *Analyst* **88,** 906–924 (1963).
65. Lowell, S., Shields, E. J., Thomas, M. a. & Thommes, M. *Characterization of Porous Solids and Powders: Surface Area, Pore Size and Density*. **16,** (2004).
66. Hurst, N. W., Gentry, S. J. & Mcnicol, B. D. Catalysis Reviews : Science and Engineering Temperature Programmed Reduction. *Catal. Letters* **24,** 233–309 (1982).
67. Wagner, C. D., Riggs, W. M., Davis, L. E. & Moulder, J. F. Handbook of X-ray Photoelectron Spectroscopy. 192 (1979). doi:10.1002/sia.740030412
68. Kelkar, C. P. & Schutz, a. a. Ni-, Mg- and Co-containing hydrotalcite-like materials with a sheet-like morphology: synthesis and characterization. *Microporous Mater.* **10,** 163–172 (1997).
69. Tanryverdiev, V. S., Aliev, O. M. & Aliev, I. I. Synthesis and physicochemical properties of cobalt aluminium hydrotalcites. *Inorganic Materials* **31,** 1497 (1995).
70. Shannon, R. D. Revised effective ionic radii and systematic studies of interatomic distances in halides and chalcogenides. *Acta Crystallogr. Sect. A* **32,** 751–767 (1976).
71. Valente, J. S., Hernandez-Cortez, J., Cantu, M. S., Ferrat, G. & L??pez-Salinas, E. Calcined layered double hydroxides Mg-Me-Al (Me: Cu, Fe, Ni, Zn) as bifunctional catalysts. *Catal. Today* **150,** 340–345 (2010).
72. Allred, A. L. & Rochow, E. G. a Scale of Electronegativity Based on Electrostatic Force. *J. lnorg. Nucl. Chem* **5,** 264–268 (1958).
73. Reichle, W. T., Kang, S. Y. & Everhardt, D. S. The nature of the thermal decomposition of a catalytically active anionic clay mineral. *J. Catal.* **101,** 352–359 (1986).
74. Meghana, S., Kabra, P., Chakraborty, S. & Padmavathy, N. Understanding the pathway of antibacterial activity of copper oxide nanoparticles. *RSC Adv.* **5,** 12293–12299 (2015).

75. Wojciechowska, M., Zielinski, M., Malczewska, A., Przystajko, W. & Pietrowski, M. Copper-cobalt oxide catalysts supported on MgF2 or Al2O3 - their structure and catalytic performance. *Appl. Catal. A-General* **298,** 225–231 (2006).
76. Stoyanova, D. *et al.* Copper-cobalt oxide spinel supported on high-temperature aluminosilicate carders as catalyst for CO-O2 and CO-NO reactions. *Appl. Catal. B Environ.* **17,** 233–244 (1998).
77. Hirose, A. *et al.* A novel metal-to-metal bonding process through in-situ formation of Ag nanoparticles using Ag2O microparticles. *Journal of Physics: Conference Series* **165,** 12074 (2009).
78. Yu, C., Li, G., Kumar, S., Yang, K. & Jin, R. Phase transformation synthesis of novel Ag2O/Ag2CO3 heterostructures with high visible light efficiency in photocatalytic degradation of pollutants. *Advanced Materials* **26,** 892–898 (2014).
79. Lucjan, C., Kustrowskia Piotr, Rafalska-Łasochaa, A. & Roman, D. Influence of Cu , Co and Ni cations incorporated in brucite-type layers on thermal behaviour of hydrotalcites and reducibility of the derived mixed oxide systems. *Thermochimica Acta* **395,** 225–236 (2003).
80. Arnoldy, P. Temperature-programmed reduction of CoO/Al2O3 catalysts. *J. Catal.* **93,** 38–54 (1985).
81. Fierro, G., Jacono, M. Lo, Inversi, M., Dragone, R. & Porta, P. TPR and XPS study of cobalt–copper mixed oxide catalysts : Evidence of a strong Co–Cu interaction. *Topics in Catalysis* **10,** 39–48 (2000).
82. XPS Interpretation of Cobalt http://www.xpsfitting.com/2012/01/cobalt.html.
83. Li, B., Xie, Y., Wu, C., Li, Z. & Zhang, J. Selective synthesis of cobalt hydroxide carbonate 3D architectures and their thermal conversion to cobalt spinel 3D superstructures. *Mater. Chem. Phys.* **99,** 479–486 (2006).
84. Swamy, C. S. Catalytic decomposition of 2-propanol on COl + xA12-xO4 spinel system. **27,** 103–112 (1994).
85. Zhu, Z. *et al.* Highly active and stable Co3O4/ZSM-5 catalyst for propane oxidation: Effect of the preparation method. *ACS Catal.* **3,** 1154–1164 (2013).
86. Salavati-Niasari, M., Mir, N. & Davar, F. Synthesis and characterization of Co3O4 nanorods by thermal decomposition of cobalt oxalate. *J. Phys. Chem. Solids* **70,** 847–852 (2009).

87. Luo, J.-Y. *et al.* Mesoporous Co3O4–CeO2 and Pd/Co3O4–CeO2 catalysts: Synthesis, characterization and mechanistic study of their catalytic properties for low-temperature CO oxidation. *J. Catal.* **254,** 310–324 (2008).
88. Torres, D. E. X-Ray Photoelectron Spectroscopy (XPS), http://www.xpsfitting.com/2013/04/silver.html. 60
89. Parres-Esclapez, S., Illàn-Gòmez, M. J., de Lecea, C. S. M. & Bueno-Lòpez, A. On the importance of the catalyst redox properties in the N2O decomposition over alumina and ceria supported Rh, Pd and Pt. *Applied Catalysis B: Environmental* **96,** 370–378 (2010).
90. Haneda, M., Kintaichi, Y., Bion, N. & Hamada, H. Alkali metal-doped cobalt oxide catalysts for NO decomposition. *Appl. Catal. B Environ.* **46,** 473–482 (2003).
91. Xue, L. I., He, H. & Liu, C. Promotion Effects and Mechanism of Alkali Metals and Alkaline Earth Metals on Cobalt - Cerium Composite Oxide Catalysts for N 2 O Decomposition. **43,** 890–895 (2009).